

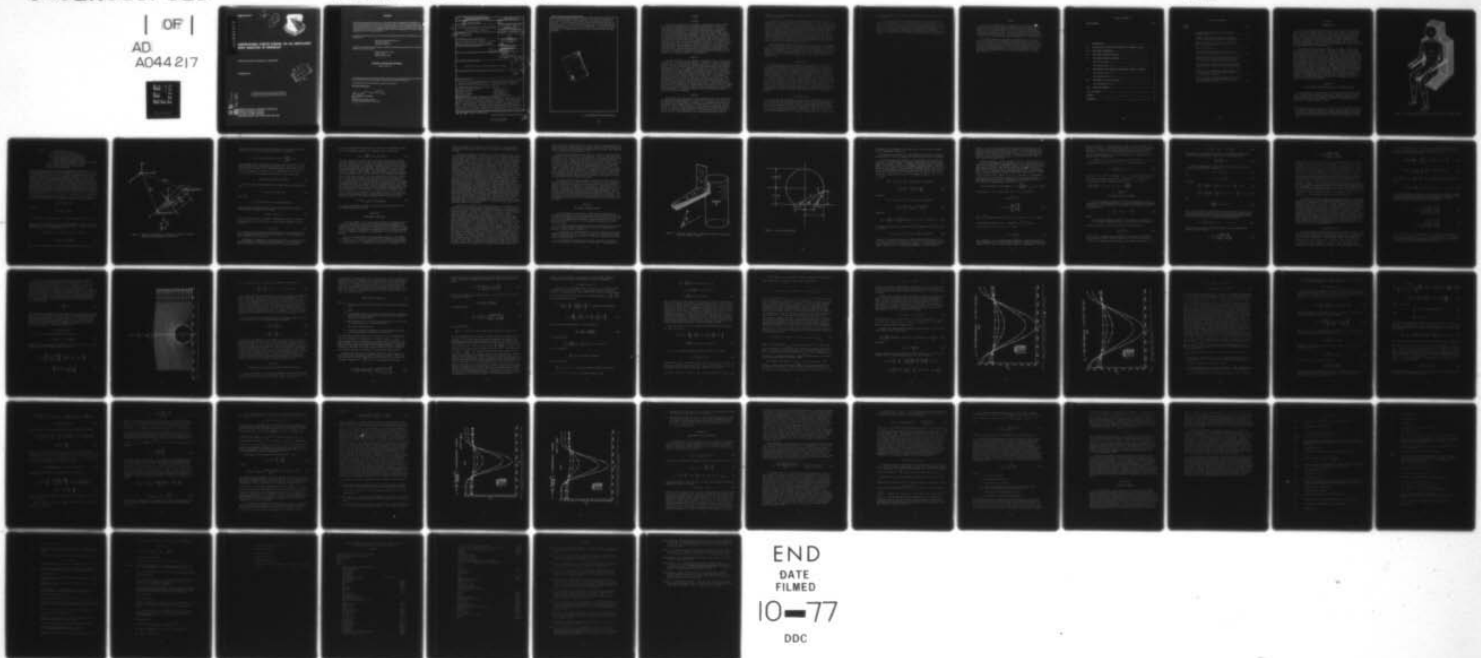
AD-A044 217

AEROSPACE MEDICAL RESEARCH LAB WRIGHT-PATTERSON AFB OHIO F/G 6/2
AERODYNAMIC FORCES EXERTED ON AN ARTICULATED BODY SUBJECTED TO --ETC(U)
DEC 76 D J SCHNECK
AMRL-TR-76-109

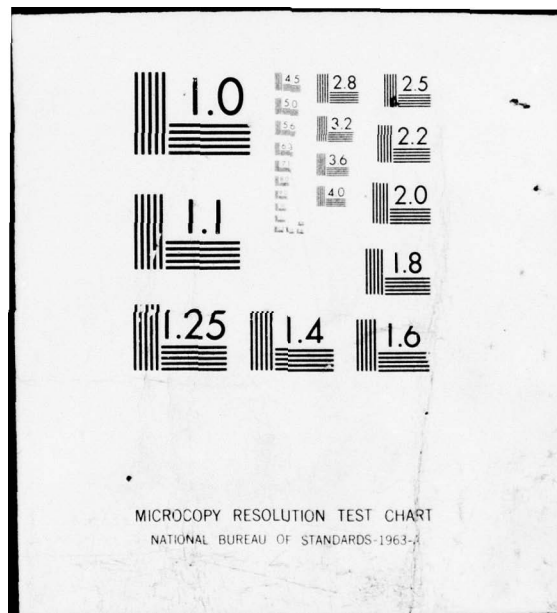
NL

UNCLASSIFIED

| OF |
AD
A044 217



END
DATE
FILMED
10-77
DDC



AMRL-TR-76-109

AD A044217

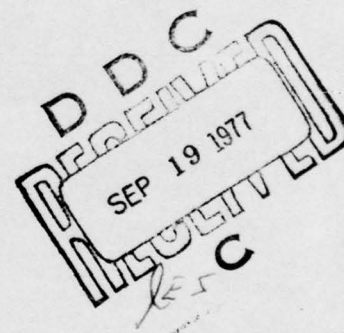
7
12



AERODYNAMIC FORCES EXERTED ON AN ARTICULATED BODY SUBJECTED TO WINDBLAST

AEROSPACE MEDICAL RESEARCH LABORATORY

DECEMBER 1976



Approved for public release; distribution unlimited

AD No. _____

DDC FILE COPY

AEROSPACE MEDICAL RESEARCH LABORATORY
AEROSPACE MEDICAL DIVISION
AIR FORCE SYSTEMS COMMAND
WRIGHT-PATTERSON AIR FORCE BASE, OHIO 45433

NOTICES

When US Government drawings, specifications, or other data are used for any purpose other than a definitely related Government procurement operation, the Government thereby incurs no responsibility nor any obligation whatsoever, and the fact that the Government may have formulated, furnished, or in any way supplied the said drawings, specifications, or other data, is not to be regarded by implication or otherwise, as in any manner licensing the holder or any other person or corporation, or conveying any rights or permission to manufacture, use, or sell any patented invention that may in any way be related thereto.

Please do not request copies of this report from Aerospace Medical Research Laboratory. Additional copies may be purchased from:

National Technical Information Service
5285 Port Royal Road
Springfield, Virginia 22161

Federal Government agencies and their contractors registered with Defense Documentation Center should direct requests for copies of this report to:

Defense Documentation Center
Cameron Station
Alexandria, Virginia 22314

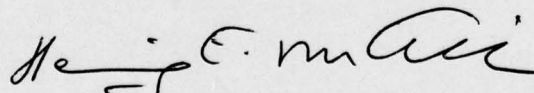
TECHNICAL REVIEW AND APPROVAL

AMRL-TR-76-109

This report has been reviewed by the Information Office (OI) and is releasable to the National Technical Information Service (NTIS). At NTIS, it will be available to the general public, including foreign nations.

This technical report has been reviewed and is approved for publication.

FOR THE COMMANDER



HENNING E. VON GIERKE
Director
Biodynamics and Bionics Division
Aerospace Medical Research Laboratory

SECURITY CLASSIFICATION OF THIS PAGE (When Data Entered)

REPORT DOCUMENTATION PAGE		READ INSTRUCTIONS BEFORE COMPLETING FORM
1. REPORT NUMBER 14 AMRL-TR-76-109	2. GOVT ACCESSION NO.	3. RECIPIENT'S CATALOG NUMBER 9
4. TITLE (and Subtitle) AERODYNAMIC FORCES EXERTED ON AN ARTICULATED BODY SUBJECTED TO WINDBLAST		5. TYPE OF REPORT & PERIOD COVERED Final Report, June 14- August 20, 1976
7. AUTHOR(s) Daniel J. Schneck*		6. PERFORMING ORG. REPORT NUMBER 14 Jan - 20 Aug 76
9. PERFORMING ORGANIZATION NAME AND ADDRESS Aerospace Medical Research Laboratory, Aerospace Medical Division, Air Force Systems Command, Wright-Patterson Air Force Base, Ohio 45433		10. PROGRAM ELEMENT, PROJECT, TASK AREA & WORK UNIT NUMBERS 61102F, 2312-V3-11
11. CONTROLLING OFFICE NAME AND ADDRESS		12. REPORT DATE December 1976
14. MONITORING AGENCY NAME & ADDRESS (if different from Controlling Office)		13. NUMBER OF PAGES 61 p.
		15. SECURITY CLASS. (of this report) Unclassified
16. DISTRIBUTION STATEMENT (of this Report) Approved for public release; distribution unlimited		15a. DECLASSIFICATION/DOWNGRADING SCHEDULE
17. DISTRIBUTION STATEMENT (of the abstract entered in Block 20, if different from Report)		
18. SUPPLEMENTARY NOTES * The author is an Associate Professor, Virginia Polytechnic Institute and State University, Blacksburg, Virginia 24061. He was in residence in AMRL as a Summer Faculty Fellow under a research associateship from the USAF/ASEE.		
19. KEY WORDS (Continue on reverse side if necessary and identify by block number) Biological and Medical Sciences Windblast Injuries Biodynamic Modeling Flail Injury Aerodynamic Forces High-Speed Ejection Inviscid Flow Theory Flow Separation Human Body Model Potential Flow Theory		
20. ABSTRACT (Continue on reverse side if necessary and identify by block number) A potential flow solution is presented for estimating the pressure distribution around the forearm of a human body subjected to windblast. The forearm is ex- amined in three positions: resting and pressing against an arm rest; resting, but not pressing against an arm rest; and not resting at all against any sur- face. Results show that a high-speed wind stream approaching the limb at some finite angle of attack has a tendency to dislodge the forearm from a surface with which it is in contact. This is due to the generation of stagnation points in the flow which lead to adverse pressure gradients as high as six times the		

DD FORM 1473 1 JAN 73 EDITION OF 1 NOV 65 IS OBSOLETE

SECURITY CLASSIFICATION OF THIS PAGE (When Data Entered)

009850

1B

/20/ free-stream dynamic pressure. Moreover, when the inviscid analysis is corrected for the effects of flow separation, it is possible to predict the presence of a pressure drag which acts to throw the forearm outward, away from the thorax. Both of these effects increase with angle of attack and they are mildly dependent on the taper of the forearm geometry. It is anticipated that a straightforward extension of the theory to other limbs of the body will shed some light on the general problem of flail injury occurring during high-speed ejections.

ACCESS N for	White Section	<input checked="" type="checkbox"/>
NTIS	B II Section	<input type="checkbox"/>
201		
14000000		
J S 100-100		
DISTRIBUTION/AVAILABILITY CODES		
SPECIAL		
A		

SUMMARY

Problem

The specific problem was to formulate a mathematical approach which will assist in predicting the aerodynamic loading to which a pilot is exposed during ejection from a high-performance aircraft. Such aerodynamic data is intended to serve as input information to the Aerospace Medical Research Laboratory's Articulated Total Body Model (ATBM), which is a further development and refinement of the Calspan model. This model, subjected to suitably defined aerodynamic loading, can be used effectively to study injuries which take place as a result of limb-flailing - that is, the tendency of the arms and legs to swing freely and out of control due to windblast forces that exceed musculoskeletal resistance. The results of the following study will also guide in planning significant wind-tunnel experiments which will provide important data for the design of high-speed ejection mechanisms. The mathematical model as developed in this report is intended to be ultimately correlated with wind-tunnel experiments in order to provide a theoretical framework from which some physical insight may be gained into the general problem of limb-flailing.

Approach

The body model used for the analysis of windblast forces in this report consists of a 15-linkage system composed of spherical, circular-cylindrical, truncated-conical and flat-plate segments attached at a series of arbitrary joints. Each of the segments can be described geometrically from available anthropometric data. Its orientation in space can, in turn, be defined by specifying the direction cosines of a coordinate system fixed to the limb, relative to an inertial coordinate system fixed in space. To illustrate the feasibility of the approach, attention has been focused specifically on the forces acting on the forearm portion of the right arm. A free stream is assumed to approach the limb at some angle of attack relative to the forearm centerline. The latter is examined in three specific positions: resting and pressing against an armrest; resting, but not pressing against an armrest; and not resting at all against any surface. For practical purposes, the stream was considered to be incompressible and inviscid, so that a stream function and velocity potential could be defined for each of the three situations described. In addition, turbulence and three-dimensional effects have been temporarily neglected.

Results

Solution of the conservation of mass and momentum equations allowed the pressure distribution around the forearm to be calculated. For the case of the forearm not resting against any surface, it was demonstrated that pressure maxima occur symmetrically at the front and back of the limb, corresponding to points of flow stagnation. These maxima decreased with angle of attack. It was also found that pressure minima occur symmetrically on the top and bottom of the forearm when it is at right angles to the incident stream, but the points themselves move leeward with decreasing angle of

attack at a rate mildly dependent on the half-angle of the truncated-cone forearm configuration.

For the case of the forearm resting against a solid surface, it was demonstrated that pressure maxima occur at the point of contact between the limb and the flat restraining plate, and that there is a high pressure region spanning nearly 160 degrees of arc along the lower half of the circular cross section. Moreover, there is a relatively deep low pressure region spanning nearly 200 degrees of arc along the top of the forearm, such that there results a rather substantial net force that acts to lift the cone (or dislodge the limb) from the surface with which it is in contact. It was also found that pressure minima occur near the top of the limb and move leeward with decreasing angle of attack at a rate mildly dependent on the cone half-angle. The net force tending to cause limb dislodgement was computed to be some six times the free stream dynamic pressure.

When the inviscid analysis was corrected for the effects of flow separation, it was possible to argue qualitatively for the existence of a profile, form or pressure drag which acts to throw the forearm outward, away from the thorax. The magnitude of this tendency is yet to be quantified, but it is in agreement with wind tunnel results which have shown a distinct upward and outward motion of the forearm when subjected to conditions similar to those simulated here.

Conclusions

It has been shown that one can approach the general problem of limb-flailing during ejection by constructing a simplified model from which the aerodynamic forces exerted on an articulated body subjected to windblast may be reasonably estimated. This model has clearly demonstrated that flow separation, together with the appearance of stagnation points in the fluid present themselves as first order effects responsible for the generation of limb-dislodging forces that result in flail injuries. The former gives rise to a pressure gradient that tends to drag the limb along with the air flow, and the latter results in a pressure gradient that tends to separate the limb from a surface with which it is in contact. Both of these effects are functions of the square of the velocity of the incident stream, and so they become rather significant at speeds near sonic. The model developed here can be progressively refined, made more sophisticated, and streamlined to provide important data for both experimental and numerical studies of human body dynamics.

Recommendations

In the early form developed thus far, the body joints themselves have not been defined, and it would be desirable to look into this in greater detail in order to assess the significance of finite length segments, end effects, three-dimensional contours and interactions which take place between the limbs as a result of their joint connections. Along the same lines, the velocity approaching any limb must be viewed as the resultant of an outer flow that has undergone specific interactions with other body segments before

it actually impinges upon the limb, and this is an area that has not yet been explored.

In refining the theory, one might also back-track to examine more closely the consequences of other assumptions made in the analysis. For example, the roughness of the surface over which the fluid flows -- which may, in part, be due to the type of clothing being worn by the pilot -- may lead to certain types of turbulent behavior that is not negligible. Similarly, at Mach numbers exceeding 0.5, compressibility effects should certainly be included and flow separation effects must be accurately quantified.

PREFACE

The work described herein was accomplished in the Mathematics and Analysis Branch of the Biodynamics and Bionics Division, Aerospace Medical Research Laboratory, Wright-Patterson Air Force Base, Ohio, during the period June 14 - August 20, 1976. At the time, the author was in residence as a Summer Faculty Fellow under a research associateship from the United States Air Force/American Society for Engineering Education, administered through the Ohio State University under the guidance of Dr. Cecil D. Bailey.

The author expresses his gratitude and appreciation to Dr. Henning E. von Gierke, Director of the Biodynamics and Bionics Division, and to Dr. Hans L. Oestreicher, Chief of the Mathematics and Analysis Branch, for their stimulating discussions, helpful guidance, continued support and warm hospitality. A special thanks to Mr. Ints Kaleps for his generous assistance and many enlightening deliberations. And a sincere "thank you" to Capt. Dave Brungart for handling all of the computer programming in connection with this study.

TABLE OF CONTENTS

SECTION NUMBER		PAGE
I.	INTRODUCTION	1
II.	THE BODY MODEL USED FOR THE ANALYSIS OF WINDBLAST FORCES	1
III.	PRELIMINARY ASSUMPTIONS	6
IV.	THE COAXAL COORDINATE SYSTEM	8
V.	THE COMPLEX VELOCITY POTENTIAL	13
	The Special Case $n = 0$	15
	The Special Case $n = 1$	17
VI.	ESTIMATION OF THE PRESSURE DISTRIBUTION AROUND THE FOREARM.....	19
	The Special Case $n = 1$	22
	The Special Case $n = 0$	29
VII.	THE EFFECTS OF FLUID VISCOSITY	37
	The Determination of C_D	39
VIII.	CONCLUDING REMARKS	41
	LIST OF SYMBOLS	43
	APPENDIX	48
	REFERENCES	50

LIST OF ILLUSTRATIONS

FIGURE NUMBER		PAGE
1	15-linkage Body Model Used For the Analysis of Windblast Forces	2
2	Schematic illustration of Forearm in relation to incident stream, including geometric description	4
3	Schematic illustration of Forearm in relation to upper arm, torso and surface of contact	9
4	Coaxial Coordinate System	10
5	Cross-Flow Streamline Pattern for Limb in contact with, but not pressing against an arm rest	18
6	Surface pressure Distribution Around Forearm having two degree angle of taper and sitting free (i.e., not in contact with any surface) in wind stream	26
7	Surface pressure Distribution Around Forearm having four degree angle of taper and sitting free in wind stream	27
8	Surface pressure Distribution Around Forearm having two degree angle of taper and resting, but not pressing against an arm rest	35
9	Surface pressure Distribution Around Forearm having four degree angle of taper and resting, but not pressing against an arm rest	36

SECTION I

INTRODUCTION

It has been estimated (Payne, 1975) that nearly half of all ejections taking place under combat conditions result in flail injury or death to the pilot. This is therefore a problem of some magnitude and it must be dealt with accordingly. In an effort to do so, the Aerospace Medical Research Laboratory of the Air Force Systems Command is pursuing experimental and analytic investigations into the dangers of ejecting a human body into a high-speed wind stream. Some preliminary experimental work in this area has already been reported (Hawker and Euler, 1975, Brinkley and Payne, 1973) and more wind tunnel tests are being planned.

The analytic studies underway at AMRL are utilizing a computerized Articulated Total Body Model (ATBM) to describe the dynamics of the human body under a variety of situations. The ATBM has grown out of the original Calspan Model (Fleck, Butler and Vogel, 1974, Bartz, 1971, Bartz and Butler, 1972) altered to include improved joint formulation, improved harness formulation and the addition of aerodynamic forces (Fleck and Butler, 1975). The latter, however, have not been clearly defined because little is known about the aerodynamic loading to which a pilot is exposed during ejection from a high performance aircraft at near sonic speeds. The work described herein was undertaken to provide some initial mathematical basis for analyzing and estimating such loading. The results are intended primarily, and ultimately to serve as input data to the ATBM Program. However, they will also guide and be correlated with corresponding wind tunnel experiments to provide a theoretical framework from which some physical insight may be gained regarding certain mechanisms which cause the limbs to swing freely and out of control, i.e., to "flail" during ejection due to windblast forces that exceed musculo-skeletal resistance.

SECTION II

THE BODY MODEL USED FOR THE ANALYSIS OF WINDBLAST FORCES

For the purposes of this analysis, the human organism has been modeled as a 15-linkage system composed of spherical, circular-cylindrical, truncated-conical and flat-plate segments attached through a series of arbitrary joints (as yet, not specifically defined).^{*} A schematic diagram of this model is shown in Figure 1, where:

^{*} The body model being developed here for the study of windblast forces differs from the ATBM in the number of segments employed and in their shape. The ATBM uses ellipsoids throughout the program for modeling the contact surfaces of the body and other curved surfaces such as interior surfaces, etc.

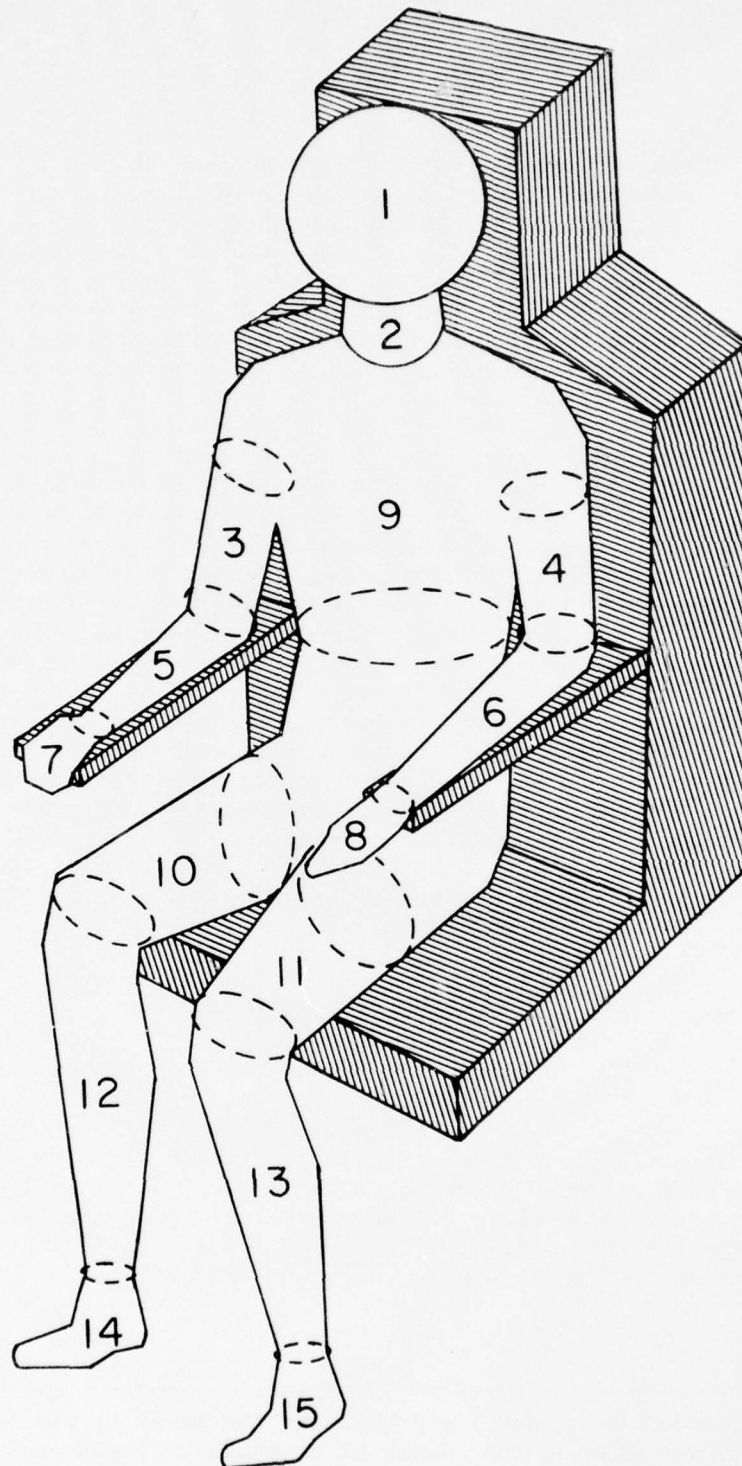


Figure 1. 15-linkage body model used for the analysis of windblast forces.

Segment	1 = Head (Sphere);
	2 = Neck (Circular Cylinder);
	3,4 = Upper Arms (Circular Cylinders);
	5,6 = Forearms (Truncated Circular Cones);
	7 = Hand Gripping Seat (Fist, Sphere);
	8 = Hand, Fingers Extended (Flat Plate);
	9 = Torso (Circular Cylinder, or Elliptic Cylinder);
	10,11 = Thighs (Truncated Circular Cones);
	12,13 = Shanks (Truncated Circular Cones);
	14,15 = Feet (Flat Plates).

Geometric description of each of the 15 segments is made possible by existing anthropometric data (Garret and Kennedy, 1971, Clauser, et al, 1972). Its respective orientation in space, in turn, is defined by specifying the direction cosines of the axes of a coordinate system fixed to the limb, relative to an inertial coordinate system fixed in space. Consider, for example, the x-y-z coordinate system fixed to the right forearm (segment 5) as illustrated in Figure 2. The x-axis is chosen to be the center-line of the truncated circular cone; the y-axis is oriented so that the free stream approaches the limb parallel to the x-y plane, and the z-axis lies perpendicular to the x-y plane. The position of the forearm may be defined at any time, t , by locating a unit vector along the x-axis relative to the inertial coordinate system, $x'-y'-z'$. Thus, if $x_1'(t)$, $y_1'(t)$ and $z_1'(t)$ represent the location of the elbow joint, and $x_2'(t)$, $y_2'(t)$ and $z_2'(t)$ represent the location of the wrist joint at any time, t , in the $x'-y'-z'$ coordinate system, then the vector from A to B along the x-axis is defined as follows:

$$\vec{r}_1(t) + \overline{AB} = \vec{r}_2(t) \quad (1)$$

from which,

$$\overline{AB} = \vec{r}_2(t) - \vec{r}_1(t),$$

or,

$$\overline{AB} = [x_2'(t) - x_1'(t)]\hat{i} + [y_2'(t) - y_1'(t)]\hat{j} + [z_2'(t) - z_1'(t)]\hat{k} \quad (2)$$

where \hat{i} , \hat{j} , and \hat{k} represent unit vectors along the x' , y' and z' directions, respectively. Now, the magnitude of the vector \overline{AB} is the square root of the sum of the squares of its components, i.e.,

$$|\overline{AB}| = \left\{ [x_2'(t) - x_1'(t)]^2 + [y_2'(t) - y_1'(t)]^2 + [z_2'(t) - z_1'(t)]^2 \right\}^{\frac{1}{2}} \quad (3)$$

Thus, a unit vector along the x-axis (the forearm centerline) relative to

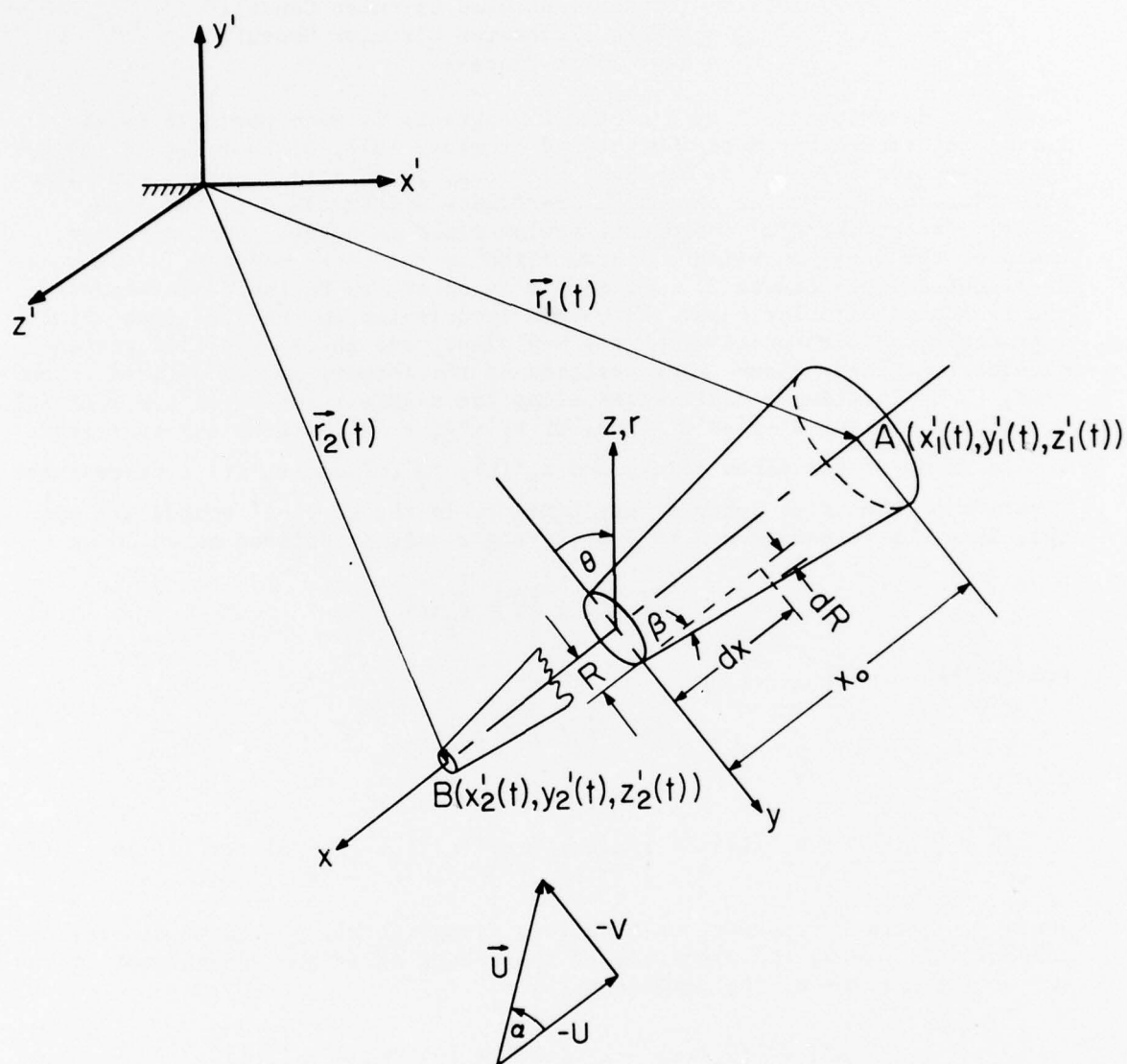


Figure 2. Schematic illustration of forearm in relation to incident stream, including geometric description.

the inertial coordinate system is given simply by equation (2) divided by equation (3), that is, the vector AB divided by its magnitude:

$$\hat{\lambda}_x = \text{unit vector from elbow to wrist} = \frac{\overline{AB(t)}}{|AB(t)|} = \hat{\lambda}_x(t). \quad (4)$$

The components of this unit vector are the direction cosines of the angle that the x-axis makes, respectively, with the x', y' and z' axes. In a similar manner, one may go on to completely describe the spatial position of any body segment, i, at any time, t, by defining the unit vectors $\hat{\lambda}_j$ (i = 1 to 15, j = x,y,z) attached to each limb at a specified joint:

$$\text{Limb position (general)} = \hat{\lambda}_j^{(i)}(t). \quad (5)$$

Now, if a free stream approaches the forearm with some constant velocity,

$$\vec{U} = U_1 \hat{i} + U_2 \hat{j} + U_3 \hat{k} = U_o \hat{\lambda}_U \quad (6)$$

such that:

$$\hat{\lambda}_U = \frac{\vec{U}}{U_o} = \text{unit vector in the stream direction}, \quad (7)$$

then the "angle of attack" between the oncoming stream and the forearm centerline may be defined to be α , where:

$$\cos \alpha(t) = \hat{\lambda}_x(t) \cdot \hat{\lambda}_U \quad (8)$$

Note, from Figure 2, that by properly orienting the y-axis, the incident stream \vec{U} can be made to lie in the x-y plane, having components -U and -V such that:

$$\tan \alpha = \frac{V}{U}. \quad (9)$$

U is then the velocity component directed parallel to the limb centerline, and V is generally referred to as the "cross-flow" velocity component in a plane perpendicular to the x-axis.

Continuing to concentrate, in this initial analysis, on the right forearm, we introduce a cylindrical coordinate system, r, θ , x as shown in Figure 2 and define the cross-sectional radius of the forearm at any

location x_0 measured from the elbow as R . Then it is clear that $R = R(x)$ and, if the forearm is modeled as a truncated right circular cone,

$$\tan \beta = \frac{dR(x)}{dx} = \text{Cone Half-Angle.} \quad (10)$$

Note that, since $R(x)$ decreases with increasing x the way the coordinate system has been set up in the limb, $\tan \beta$ as defined by equation (10) is negative. Similarly, $\tan \alpha$ as defined by equation (9) is positive, since V and U are both assumed to be negative. Finally, the angle θ is considered positive when measured counterclockwise from the positive y -axis. As mentioned previously, the parameters β (cone half-angle), l (total forearm length from elbow to wrist = $|AB|$), $R(x)$ and others pertinent to the geometric description of the limb may be deduced from available anthropometric data for adult men and women. The free stream velocity, \vec{U} refers specifically to the velocity approaching the forearm "as the forearm sees it," i.e., including the effects of the presence of a torso and other wind-deflecting disturbances. It is thus intimately coupled with the flow regimes surrounding the other body segments and its determination must necessarily involve solving an entire complex system of equations simultaneously. This matter shall be dealt with in greater detail during a subsequent phase of this investigation. For the present, we assume only the simplest case - that is, that \vec{U} is the resultant of the average velocity of the pilot with respect to the plane during the ejection phase plus the velocity of the plane with respect to the inertial reference frame (e.g., the ground):

$$\vec{U} = \vec{U}_{\text{pilot/plane}} + \vec{U}_{\text{plane/ground}} \quad (11)$$

Some additional comments relative to equation (11) shall be made in the Concluding Remarks (Section VIII).

SECTION III

PRELIMINARY ASSUMPTIONS

In the most general sense, this problem involves the turbulent flow of a viscous, compressible fluid around a complicated three-dimensional 15-linkage system of finite bodies of revolution attached at undefined joints. Obviously, one must begin modestly by making significant simplifying assumptions if any degree of mathematical tractability is to be sought in getting an order of magnitude estimate of the aerodynamic forces with which we are dealing.

The first assumption which clearly simplifies matters is the neglect of turbulence, i.e., the flow is considered to be laminar except, perhaps, in a finite region on the downstream side of the bluff body segments where flow separation occurs. The laminar-flow hypothesis is introduced for the

sake of convenience. Its validity can be evaluated by comparing analytic results with experimental data, which will be done as such data becomes available.

The second assumption is certainly more controversial, but has led to some surprisingly meaningful results when applied to analogous flow patterns over slender inclined bodies of revolution (see, for example, Allen and Perkins, 1951, Kelly, 1954 and Mello, 1959). That is, it shall be assumed for the moment that the effects of viscosity in the fluid may be linearly super-imposed on the inviscid flow solutions, such that the latter may be determined as if they were completely independent of any surface viscous effects. Looking at the problem in greater detail, one observes that this assumption is probably not as bad as it may sound. In general, during the early stages of flow development around a blunt body of revolution, the vorticity in the fluid is practically confined to the boundary layer and to the separated wake region behind the body (Goldstein, 1938, page 61). Now in a very high Reynolds number flow the laminar boundary layer can be expected to be quite thin, and, during the first few milliseconds of flow development, thinner still because not much time has elapsed to allow the boundary layer to grow. It thus seems likely that during this time the wake region dominates the flow patterns to a much greater extent than do any effects taking place in the growing surface boundary layer itself. In fact, even in fully-developed flow situations over bluff bodies, the skin-friction drag is small compared with the form drag, or pressure drag, due to flow separation (Goldstein, 1938, page 65). Considering that the problem being dealt with here is one of very high Reynolds number (near sonic velocities of air the Reynolds number is of order 10^6), and that most flail injuries take place within the first 3 milliseconds of the ejection process, it would seem that, for practical purposes, the flow up to the point of boundary-layer separation may be considered to be inviscid without destroying the essential physics of the problem.

Going one step further, the pressure drag due to flow separation may be accounted for by a super-position of inviscid solutions - if the boundary layer on the surface of the body is neglected following the reasoning of the previous paragraph. Consider, for example, the case of a circular cylinder placed so that its axis is at a right angle to an oncoming stream. Goldstein (1938, page 60) points out that when the flow is started from rest, separation of the boundary layer begins at the rear of the cylinder after a period of time that is roughly proportional to the radius and inversely proportional to the speed of the outer flow. At 600 miles per hour, this would correspond to t of order 10^{-4} seconds for the cylindrical segments characteristic of the body model depicted in Figure 1. Thus, for all intents and purposes, it may be postulated that separation of the flow takes place at all limbs almost instantaneously at the start of the ejection process near sonic speeds. Moreover, during the first 3 milliseconds of flow development, the separated wake stays confined to the immediate region of the cylinder, and consists essentially of two thin vortex-layers, symmetrically situated. It is thus possible to model this situation analytically by simply super-imposing stationary vortex filaments upon the linear solution for inviscid flow past a cylinder (see Milne-Thomson, 1960, pages 367-369 and Mello, 1959). What one obtains is a reasonable estimate of the pressure distribution along the surface of the cylinder, and pressure forces are

those of greatest concern during the catapult phase of high-speed ejections. Going back to the assumption, then, one must conclude that it is feasible to begin this analysis by examining and super-imposing potential flow solutions for the geometries shown in Figures 1 and 2.

The third major assumption which shall be inherent in this preliminary formulation is that the flow is two-dimensional. That is, end effects and conditions at the joints of the body model will be temporarily neglected and the outer flow as it approaches the limb will not be considered to be a function of x , the coordinate along the limb centerline. As can the assumption that follows, this one may be subsequently modified by introducing "correction factors" to account for three-dimensional effects (see, for example, Goldstein, 1938, page 439, where he discusses cylinders of finite span). In any case, the consequences of assuming a relatively large aspect ratio (length to average diameter) for the limbs should be to predict somewhat higher drag forces than are actually manifest. Effects at the ends of finite-span elements tend to alter the separated flow patterns in such a way that profile drag is actually decreased.

The fourth, and final major assumption which will be made is that the flow is incompressible. Like the neglect of turbulence, this assumption is clearly arbitrary at this point and, considering that the ejection Mach number is near unity, probably not a very good one. Nevertheless, it may be possible to include the effects of compressibility through the use of correction factors based on the results of wind tunnel experiments. There is some data available which presents various coefficients of drag, lift, etc. as functions of the mean free-stream Reynolds number and Mach number. Perhaps such data can be incorporated into this analysis at a later time. For the present, assuming the flow to be incompressible certainly simplifies the mathematics.

SECTION IV

THE COAXIAL COORDINATE SYSTEM

In the remainder of this report, we shall show the feasibility of analyzing the aerodynamic forces exerted on an articulated body subjected to windblast by focusing specific attention on the forearm portion of the right arm. This body segment was discussed in some detail (Section III) with reference to Figures 1 and 2, and we now propose to examine the limb in three positions:

- 1) resting and pressing against an arm rest, such that there is a flat surface of contact between forearm and seat rest (this configuration is depicted in cross-section in Figure 4);
- 2) resting but not pressing against an arm rest, such that the contact between forearm and seat rest is just a straight line element of both surfaces (this configuration is illustrated in Figure 1, and magnified schematically in Figure 3); and,
- 3) not resting at all against any surface, such that the forearm behaves essentially as a slender body in a free stream - disregarding, for

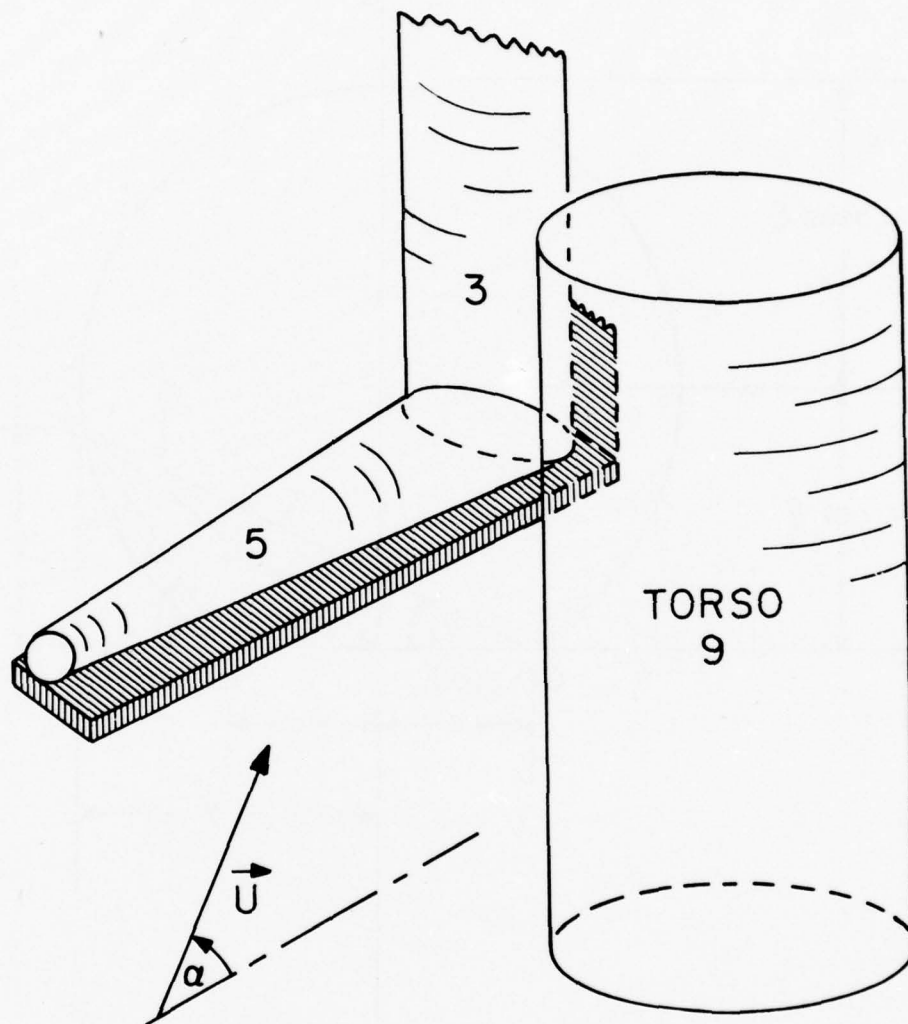


Figure 3. Schematic illustration of forearm in relation to upper arm, torso and surface of contact.

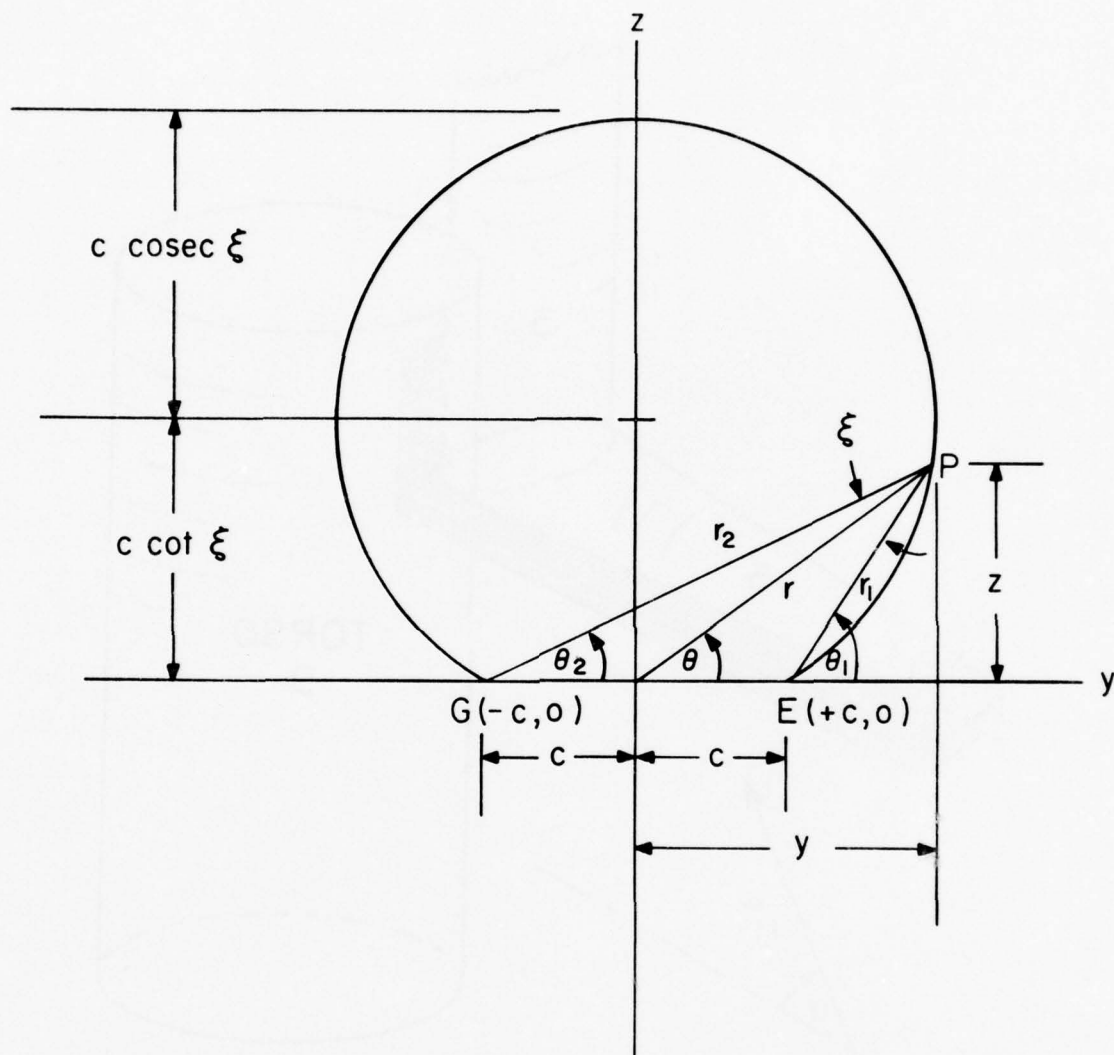


Figure 4. Coaxial coordinate system.

the moment, its attachment to the other parts of the body (this configuration is illustrated in Figure 2).

The above three positions are representative of some which are typical during ejection. There are others, but they have not as yet been examined.

In order to pursue the analysis, it is convenient, at this point, to introduce a so-called "coaxial" coordinate system (see Milne-Thomson, 1960, page 171), depicted in Figure 4. Consider an arbitrary point, P, in the y-z plane. The location of P in the rectangular coordinate system is given by the point (y,z), while in the cylindrical coordinate system, it is the point (r,θ). We now define two points, G(-c,0) and E(+c,0) on the y-axis as shown, and locate point P as the intersection of the lines r₂ and r₁ drawn respectively through points G and E at the angles θ₂ and θ₁. Let ξ = θ₁ - θ₂. Then:

$$\begin{aligned}\sin \xi &= \sin (\theta_1 - \theta_2) = \sin \theta_1 \cos \theta_2 - \cos \theta_1 \sin \theta_2 \\ &= \frac{z}{r_1} \frac{y+c}{r_2} - \frac{y-c}{r_1} \frac{z}{r_2} = \frac{2zc}{r_1 r_2}\end{aligned}\quad (12)$$

Similarly,

$$\begin{aligned}\cos \xi &= \cos (\theta_1 - \theta_2) = \cos \theta_1 \cos \theta_2 + \sin \theta_1 \sin \theta_2 \\ &= \frac{y-c}{r_1} \frac{y+c}{r_2} + \frac{z}{r_1} \frac{z}{r_2} = \frac{y^2 - c^2 + z^2}{r_1 r_2}\end{aligned}\quad (13)$$

Therefore,

$$\cot \xi = \frac{\cos \xi}{\sin \xi} = \frac{y^2 - c^2 + z^2}{2zc}, \text{ and, } y^2 - c^2 + z^2 - 2zc(\cot \xi) = 0. \quad (14)$$

If we add and subtract the quantity c²cot²ξ to equation (14), it may be put in the form:

$$[z - c(\cot \xi)]^2 + y^2 = c^2(1 + \cot^2 \xi) = c^2 \operatorname{cosec}^2 \xi. \quad (15)$$

Equation (15) is precisely that of a circle centered at the point y = 0, z = c(cot ξ), having a radius equal to c(cosec ξ). The intersection of this circle with the line z = 0 is the chord line GE. In cross-section, then, Figure 4 appears to be a suitable representation for case 1 described

earlier, i.e., the forearm resting and pressing against an arm rest. The forearm cross-section is defined by the circle $\xi = \text{constant}$ and the flat surface of contact between forearm and seatrest ($z = 0$) is defined by the chord GE, or the points $(+c, 0)$, $(-c, 0)$. By varying c , we may change the extent of contact, GE, while adjusting ξ so that the quantity $c(\text{cosec } \xi)$ stays within physiologic limits.

Note that $c(\text{cosec } \xi) = c(\cot \xi)$ when $\xi = 0, 2\pi, \dots, 2n\pi$ ($n = 0, 1, 2, \dots$) so that these represent the limiting case of the circle tangent to the y-axis at the point $(0, 0)$. Furthermore, when $\xi = 0$, c must also be zero to keep $c(\text{cosec } \xi)$ finite. This reduces chord GE to the point $(0, 0)$ which is consistent with the fact that the circle becomes tangent to the y-axis. Thus, $\xi = 0$ is a convenient way to represent case 2, i.e., the arm resting but not pressing against an arm rest. Note further that $c(\cot \xi) = 0$ (for finite c) when $\xi = (2n + 1)\frac{\pi}{2}$ ($n = 0, 1, 2, \dots$) so that $\xi = \frac{\pi}{2}$ represents the limiting case of the circle centered at the point $(0, 0)$ of radius c . We shall show later that this is a convenient way to represent case 3, i.e., the forearm not resting against any surface at all.

Let us now define a second quantity, $\eta = \ln \left[\frac{r_2}{r_1} \right] = \ln r_2 - \ln r_1$, so that

we may write: $\eta - i\xi = \ln r_2 + i\theta_2 - \ln r_1 - i\theta_1 = \ln (r_2 e^{i\theta_2})$

$- \ln (r_1 e^{i\theta_1})$, or,

$$\eta - i\xi = \ln \left(\frac{r_2 e^{i\theta_2}}{r_1 e^{i\theta_1}} \right). \quad (16)$$

Now, $r_2 e^{i\theta_2}$ may be written as $(y + c) + iz = (y + iz) + c = \chi + c$, where χ

is the complex variable $(y + iz)$. Similarly, $r_1 e^{i\theta_1} = r_1 \cos \theta_1$

$+ r_1(i \sin \theta_1) = (y - c) + iz = \chi - c$. Thus,

$$e^{\eta - i\xi} = \frac{\chi + c}{\chi - c}. \quad (17)$$

The coordinates η, ξ are called Coaxal coordinates. Equation (15) has already revealed that $\xi = \text{constant}$ yields a family of circles centered at the point $y = 0$, $z = c(\cot \xi)$, with radius $c(\text{cosec } \xi)$, c being given. It can be

shown further that $\eta = \text{constant}$ yields a family of circles centered at the point $y = c(\coth \eta)$, $z = 0$, having radii equal to $c(\text{cosech } \eta)$. Any point P may thus be defined in the coaxial coordinate system as the intersection of two circles, ξ_0 and η_0 . The discussion earlier, and the material which follows indicate that the use of coaxial coordinates is convenient for the problem being considered here.

To complete this section, we define the complex variable $\zeta = \xi + i\eta$. From equation (17), then, $e^{-i\zeta}(\chi - c) = \chi + c$, from which we get:

$$\frac{\chi}{c} = \frac{e^{-i\zeta} + 1}{e^{-i\zeta} - 1} = i \cot \frac{\zeta}{2} \quad (18)$$

Thus, $\chi = y + iz = re^{i\theta} = ic[\cot \frac{\zeta}{2}]$; $\zeta = \xi + i\eta$. From these relations, one may invert the process to get y and z as functions of c , ξ and η ; we may also define the complex conjugate functions: $\bar{\chi} = y - iz = re^{-i\theta} = -ic[\cot \frac{\bar{\zeta}}{2}]$, $\bar{\zeta} = \xi - i\eta$, $\xi = \theta_1 - \theta_2$, $\eta = \ln \left[\frac{r_2}{r_1} \right]$.

SECTION V

THE COMPLEX VELOCITY POTENTIAL

For the two-dimensional laminar flow of an incompressible fluid, the conservation of mass requirement may be identically satisfied by introducing the concept of a stream function, ψ , such that, in a rectangular cartesian coordinate system,

$$u = - \frac{\partial \psi}{\partial z} \quad \text{and,} \quad v = \frac{\partial \psi}{\partial y} \quad (19)$$

where:

u = the velocity component parallel to the y -axis, at the point y, z ,
 v = the velocity component parallel to the z -axis, at the point y, z ,

and the conservation of Mass (Continuity) equation is given by:

$$\frac{\partial u}{\partial y} + \frac{\partial v}{\partial z} = 0. \quad (20)$$

If the fluid is considered to be inviscid as well, then it is possible to show that there exists a potential function, ϕ , such that the velocity vector, \vec{v} , has components corresponding to the negative gradient of ϕ , i.e.,

$$u = -\frac{\partial \phi}{\partial y} \quad \text{and,} \quad v = -\frac{\partial \phi}{\partial z}. \quad (21)$$

Substitution of the expressions (21) into the Continuity equation (20) yields the well-known Laplace equation for the determination of ϕ :

$$\frac{\partial^2 \phi}{\partial y^2} + \frac{\partial^2 \phi}{\partial z^2} = 0. \quad (22)$$

Under the assumptions of Section III, therefore, we may introduce a complex velocity potential, w , given by:

$$w = \phi + i\psi = w(\chi) \quad (23)$$

and

$$\bar{w} = \phi - i\psi = \bar{w}(\bar{\chi}) \quad (24)$$

such that:

$$-\frac{\partial w}{\partial z} = -\frac{dw}{d\chi} \frac{\partial \chi}{\partial z} = -\frac{dw}{d\chi} (i) = v + iu, \quad \frac{dw}{d\chi} = -u + iv \quad (25)$$

$$+\frac{\partial \bar{w}}{\partial z} = +\frac{d\bar{w}}{d\bar{\chi}} \frac{\partial \bar{\chi}}{\partial z} = +\frac{d\bar{w}}{d\bar{\chi}} (-i) = -v + iu, \quad \frac{d\bar{w}}{d\bar{\chi}} = -u - iv \quad (26)$$

Thus,

$$\frac{dw}{d\chi} \frac{d\bar{w}}{d\bar{\chi}} = u^2 + v^2 = q^2 \quad (27)$$

where q^2 is the square of the magnitude of the fluid velocity at any point. The complex velocity potential for the cross-flow in this problem may be deduced from the form of the coaxial coordinate system defined by equation (18) of Section IV. That is, consider the complex potential:

$$w = V \frac{2ci}{n} \cot \frac{\zeta}{n} = \phi + i\psi, \quad \zeta = \xi + i\eta \quad (28)$$

Expanding this potential, and separating the real and imaginery parts yields, after some algebra:

$$\phi = V \frac{2c}{n} \frac{\tanh\left(\frac{\eta}{n}\right) \sec^2\left(\frac{\xi}{n}\right)}{\tan^2\left(\frac{\xi}{n}\right) + \tanh^2\left(\frac{\eta}{n}\right)} \quad (29)$$

$$\psi = V \frac{2c}{n} \frac{\tan\left(\frac{\xi}{n}\right) \operatorname{sech}^2\left(\frac{\eta}{n}\right)}{\tan^2\left(\frac{\xi}{n}\right) + \tanh^2\left(\frac{\eta}{n}\right)} \quad (30)$$

Multiplying the top and bottom of equations (29) and (30) by the quantity $\cos^2\left(\frac{\xi}{n}\right)$ reveals that ϕ remains finite, whereas ψ goes to zero if $\xi = 0$ (n finite) and $\xi = n\frac{\pi}{2}$ ($n \neq 0$). Now, the limiting stream function, $\psi = 0$ defines the geometric configuration of an obstacle disturbing the cross-flow of velocity V . Thus, consider what this configuration is for $\xi = n\frac{\pi}{2}$. We have already seen (from equation (15) of section IV) that, for c given, $\xi = \text{constant}$ defines circles that intercept the y -axis at the points $\pm c$. In particular, then, $\xi = n\frac{\pi}{2}$ defines such circles for various values of the parameter n (except $n = 0$, which must be treated as a special case because ϕ and ψ as defined by equations (29) and (30) are undefined for this value of n). Furthermore, the degenerate case, $\xi = 0$, $n \neq 0$ is clearly that portion of the y -axis lying outside the points $\pm c$, for $\xi = \theta_1 - \theta_2 = 0$ when $\theta_1 = \theta_2 = 0$ (positive y -axis to the right of point $+c$ on Figure 4) and $\xi = \theta_1 - \theta_2 = 0$ when $\theta_1 = \theta_2 = 180^\circ$ (negative y -axis to the left of point $-c$).

To summarize, we find that the complex velocity potential (28) defines exactly the cross-flow over a geometric configuration such as that depicted in Figure 4, corresponding to case (1) of the forearm-seat-rest interactions being considered here. That is, the limiting streamline $\psi = 0$ defines the arm-rest y -axis outside the points $\pm c$, together with the circular arm intersecting the y -axis at the points $\pm c$. We may point out further that the same velocity potential would also define the flow of a fluid past a configuration which consisted of that shown in Figure 4, together with its mirror image on the other side of the y -axis. In other words, if a second cylinder were placed on the negative z side of Figure 4, such that it shared a common base GE with the cylinder shown, then the complex velocity potential (28) would characterize that flow situation as well. This has direct relevance to the problem of one limb pressing against another, which is merely an extension of the theory being developed here.

The Special Case $n = 0$

It was already mentioned in Section III that if we wish to keep $c(\operatorname{cosec} \xi)$, the radius of the circle shown in Figure 4, finite as $\xi \rightarrow 0$, then c must also go to zero, reducing the chord GE to the point $(0,0)$ and making the circle tangent to the y -axis. In the present context, this means that c should go to zero as n (and hence, $\xi = n\frac{\pi}{2}$) does, reducing the problem to flow around a cylinder tangent to the y -axis, which corresponds to the cross-section of case (2) shown in Figure 3. Note from equation (18) that

if χ is to remain finite as c goes to zero, then $\tan\left(\frac{\zeta}{2}\right)$ should also go to zero with c , indicating that ζ , too, becomes very small with n . For small c , n and ζ , we may therefore write:

$$\chi = ic \left[\cot \left(\frac{\zeta}{2} \right) \right] = ic \frac{\cos \frac{\zeta}{2}}{\sin \frac{\zeta}{2}} \approx ic \frac{1}{\frac{\zeta}{2}} = \frac{2ic}{\zeta}, \text{ or, } \zeta = \frac{2ic}{\chi} \quad (31)$$

$$c(\operatorname{cosec} \xi) = \frac{c}{\sin \frac{\pi}{2}} \approx \frac{c}{\frac{n\pi}{2}} = \frac{2c}{n\pi} = a = \text{radius of circle} \quad (32)$$

and so, $\frac{2ci}{n} = \pi ai$, $\frac{\zeta}{n} = \frac{2ic}{\chi n} = \frac{\pi ai}{\chi}$, which, substituted into equation (28), gives:

$$w = V(\pi ai) \cot \frac{\pi ai}{\chi} = \pi aV \coth \frac{a\pi}{\chi} = \phi + i\psi, \quad \chi = y + iz \quad (33)$$

as the complex velocity potential for cross-flow past a cylinder of radius "a" and axis parallel to x , tangent to the x - y plane. Once again, expanding equation (33) and separating the real and imaginery parts yields the velocity potential and stream function for the motion:

$$\phi = \pi aV \frac{\tanh \frac{a\pi y}{2} \sec^2 \frac{a\pi z}{2}}{\tanh^2 \frac{a\pi y}{2} + \tan^2 \frac{a\pi z}{2}} \quad (34)$$

$$\psi = \pi aV \frac{\tan \frac{a\pi z}{2} \operatorname{sech}^2 \frac{a\pi y}{2}}{\tanh^2 \frac{a\pi y}{2} + \tan^2 \frac{a\pi z}{2}} \quad (35)$$

where: $r^2 = y^2 + z^2$ and the streamline $\psi = 0$ consists of the boundary $z = 0$ (the real axis) and the circle $y^2 + z^2 = 2az$ centered at $z = a$ and tangent to the real axis at $(0,0)$. The latter is obtained in analytic form from equation (15), using the approximations (31) and (32).

Equation (35) has been programmed (Appendix) and Figure 5 shows a typical cross-flow streamline pattern for the arbitrary case of $a = V = 1$ which essentially non-dimensionalizes the stream function ψ . Note, in particular, the stagnation point at $y = 0, z = 0$ and the relatively high velocity (proportional to the distance between streamlines) at $y = 0, z = 2$. This indicates, as will be shown more rigorously later on, that the pressure at the base of the cylinder is much higher than it is on top of the cylinder, so that there is a tendency to "lift" it from the surface with which it is in contact. Note, also, that the streamline pattern evens out to a nearly parallel, uniform distribution as we move further and further away from the cylinder. In fact, if we take the limit of equation (33) as $\chi \rightarrow \infty$, we find that:

$$w \rightarrow \frac{\pi a V}{\chi} = V \chi \quad (36)$$

which is exactly the complex velocity potential for a uniform stream, moving from right to left parallel to the real axis. As an interesting side-light, we might also mention that the complex potential (36) can be deduced from equations (18) and (28) as the special case for $n = 2$, so that the latter represents infinitely unbounded flow parallel to the real plane in the absence of an obstacle. This has no immediate relevance to the problem at hand, but constitutes an interesting observation.

The Special Case $n = 1$

For $n = 1$, the complex potential (28) reduces to:

$$w = 2ciV \cot \zeta = 2ciV \frac{\cos \zeta}{\sin \zeta} \quad (37)$$

Making use of the trigonometric identities for the sine and cosine of double angles, we may re-write equation (37) as follows:

$$\begin{aligned} w &= 2ciV \left[\frac{\cos^2 \frac{\zeta}{2} - \sin^2 \frac{\zeta}{2}}{2 \sin \frac{\zeta}{2} \cos \frac{\zeta}{2}} \right] = V \left[ic \left(\cot \frac{\zeta}{2} \right) - ic \left(\tan \frac{\zeta}{2} \right) \right] \\ &= V \left[ic \left(\cot \frac{\zeta}{2} \right) + \frac{c^2}{ic \left(\cot \frac{\zeta}{2} \right)} \right] \end{aligned} \quad (38)$$

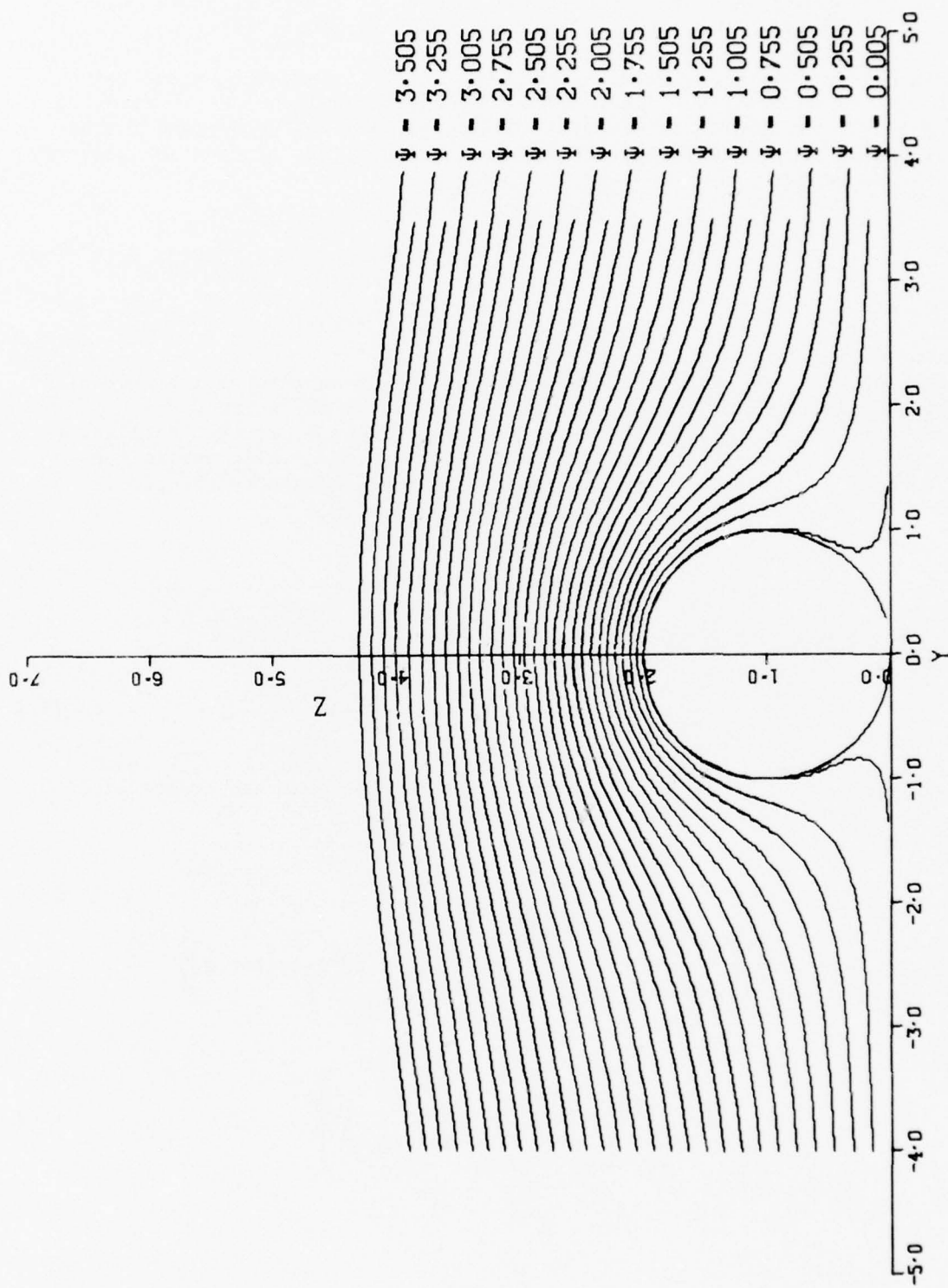


Figure 5. Cross-flow streamline pattern for limb in contact with, but not pressing against an arm rest.

But, from equation (18), $ic \left(\cot \frac{\zeta}{2} \right) = \chi$, so equation (38) reduces to:

$$w = V \left[\chi + \frac{c^2}{\chi} \right] = \phi + i\psi, \quad \chi = y + iz = re^{i\theta} \quad (39)$$

which is precisely the complex velocity potential for uniform streaming past a free cylinder of radius c oriented with its axis perpendicular to the flow. This, then, corresponds to the cross-flow at a station x of case (3) which we are examining and which is depicted in Figure 2 (note that the velocity V is perpendicular to the cone axis, x). It is now clear that the coaxial coordinate system, and the complex potential (28) are particularly useful for describing the cross-flow in each of the three configurations under investigation in this study. In fact, they can be used to describe a variety of other configurations as well - for example - one limb in contact with another as discussed at the end of the section dealing with the case $n = 0$.

As has been done in previous sections, we now expand equation (39) and separate it into its real and imaginary parts to obtain:

$$\phi = V \left[r + \frac{c^2}{r} \right] \cos \theta \quad (40)$$

$$\psi = V \left[r - \frac{c^2}{r} \right] \sin \theta \quad (41)$$

At this point, the complex velocity potential, stream function and potential function have been deduced for each of the three basic configurations depicted in Figures 2, 3 and 4. They are, respectively, equations (28), (29) and (30) for Figure 4, corresponding to case 1 (forearm pressing against seat rest handle); equations (33), (34) and (35) for Figure 3, corresponding to case 2 (forearm just touching, i.e., tangent to seat rest handle); and, equations (39), (40) and (41) for Figure 2, corresponding to case 3 (forearm freely exposed to oncoming stream). In the section that follows, these velocity functions shall be used to estimate the pressure distribution around the forearm in each configuration, and we shall see how the angle of attack, α , and the cone half-angle, β , enter into the analysis.

SECTION VI

ESTIMATION OF THE PRESSURE DISTRIBUTION AROUND THE FOREARM

The stream function, ψ , and velocity potential, ϕ , have both been shown to satisfy the conservation of mass equation (20). In order to uniquely define the fluid motion, however, we must also satisfy conservation

relationships for momentum and energy. The latter two become uncoupled from one another under the assumption of incompressibility, and it thus becomes possible, for an inviscid fluid, to solve directly for the pressure distribution once ϕ is obtained from equation (22). The procedure involves the solution of an integrated form of the conservation of momentum equation, where the integration is performed along a streamline ($\psi = \text{constant}$) of the flow. The result is the well-known Bernoulli equation, which, neglecting body forces, takes the form:

$$-\frac{\partial \phi}{\partial t} + \frac{q^2}{2} + \frac{p}{\rho} = \text{Constant}, C_o \quad (42)$$

where:

ϕ = the local cross-flow velocity potential, determined from equation (22);

t = time;

q^2 = the magnitude squared of the local fluid velocity at a specified point in the flow, as determined by equation (27) utilizing the complex velocity potential;

p = the pressure due to cross-flow at the same point as that at which q^2 is determined, for a corresponding time, t ;

ρ = the fluid mass density; and,

C_o = a constant, generally determined from known ambient conditions, or from conditions at a known point in the flow.

The integrated momentum equation (42) is obviously a form of energy equation, as evidenced by the appearance of a kinetic energy term, $\frac{1}{2} \rho q^2$, a pressure energy term, p (proportional to molecular kinetic energy per unit mass of fluid), and so on (potential energy terms also appear if body and field forces are taken into account in the momentum equation). Thus, the constant C_o represents the "total" energy of the flow along a streamline, which remains constant in the absence of dissipating viscous effects.

Equation (42) may be used to estimate the pressure distribution for each of the three configurations shown in Figures 2, 3 and 4. Thus, consider the complex velocity potential given by equation (28), together with its complex conjugate, $\bar{w} = -V \frac{2ci}{n} \cot \frac{\bar{\zeta}}{n}$. From equation (27) we have:

$$q^2 = \frac{dw}{d\chi} \frac{d\bar{w}}{d\bar{\chi}} = \frac{dw}{d\zeta} \frac{d\bar{w}}{d\bar{\zeta}} \frac{d\zeta}{d\chi} \frac{d\bar{\zeta}}{d\bar{\chi}} = \frac{16V^2}{n^4} \left(\frac{\sin \frac{\zeta}{2} \sin \frac{\bar{\zeta}}{2}}{\sin \frac{\zeta}{n} \sin \frac{\bar{\zeta}}{n}} \right)^2 \quad (43)$$

where the derivatives are obtained from equations (28), (18) and their respective conjugates. Expanding, rearranging and simplifying equation (43) yields:

$$q^2 = \frac{16V^2}{n^4} \left\{ \frac{\cosh \eta - \cosh \xi}{\cosh \frac{2\eta}{n} - \cos \frac{2\xi}{n}} \right\}^2 \quad (44)$$

which is the second term of equation (42). We can also use the chain rule of calculus to write:

$$\frac{\partial \phi}{\partial t} = \frac{\partial \phi}{\partial c} \frac{\partial c}{\partial t} = \frac{\partial \phi}{\partial c} \frac{dc}{dx} \frac{dx}{dt} \quad (45)$$

From equation (29):

$$\frac{\partial \phi}{\partial c} = \frac{\partial}{\partial c} \left\{ V \frac{2c}{n} \frac{\tanh\left(\frac{\eta}{n}\right) \sec^2\left(\frac{\xi}{n}\right)}{\tan^2\left(\frac{\xi}{n}\right) + \tanh^2\left(\frac{\eta}{n}\right)} \right\} \quad (46)$$

Also, by definition:

$$\frac{dx}{dt} = -U = -U_0 \cos \alpha = \text{the stream velocity parallel to the x-axis.}$$

The quantity $\frac{dc}{dx}$ defines the surface of contact between the forearm and the seat rest. It is finite when the forearm configuration is taken to be a truncated cone, and its value depends upon β , the cone half-angle, and n , which determines the "degree" or extent of pressing (i.e., contact) between forearm and arm rest. In fact, we may write: $\frac{dc}{dx} = \frac{dc}{dn} \frac{dn}{dx}$, where $\frac{dc}{dn} = f(n)$ indicates how the chord line GE (Figure 4) varies with n - hence the extent of contact - and $\frac{dn}{dx} = f(\beta)$ indicates how the chord line GE varies with x - hence the half-angle of the forearm truncated cone configuration. Specification of these quantities, together with U_0 , the angle of attack, α , and equation (46) allow equation (45) to be evaluated, which then determines the first term of equation (42). Adding appropriate ambient information allows C_0 to be computed. Thus, combining equations (44), (45) and (42) with C_0 known, we may solve for p , the pressure distribution on the surface of the forearm as a function of several variables - which include forearm geometry, degree of forearm/seat rest contact, free-stream conditions and the manner in which the stream approaches the limb. Obviously, the solution process becomes quickly complicated and computer methods must be employed to handle the mathematics in a convenient fashion. For illustrative purposes,

however, we may go directly to two specific cases in order to show the feasibility of the approach and continue the analytic development.

The Special Case $n = 1$

The easiest case to examine first is case 3 ($n = 1$) of Figure 2, where the forearm is depicted as a free, tapered slender body at an angle of attack to an oncoming stream. Thus, consider the complex velocity potential given by equation (39), together with its complex conjugate, $\bar{w} = V \left[\bar{\chi} + \frac{c^2}{\bar{\chi}} \right]$. From equation (27), we have:

$$q^2 = \frac{dw}{d\chi} \frac{d\bar{w}}{d\bar{\chi}} = V \left[1 - \frac{c^2}{\chi^2} \right] V \left[1 - \frac{c^2}{\bar{\chi}^2} \right], \text{ or, expanding and rearranging}$$

$$q^2 = V^2 \left[\left(1 - \frac{c^2}{r^2} \right)^2 \cos^2 \theta + \left(1 + \frac{c^2}{r^2} \right)^2 \sin^2 \theta \right]. \quad (47)$$

Equation (45) now becomes, since $c = R(x)$ in Figure 2:

$$\frac{\partial \phi}{\partial t} = \frac{\partial \phi}{\partial c} \frac{\partial c}{\partial t} = \frac{\partial \phi}{\partial R} \frac{dR}{dx} \frac{dx}{dt} \quad (48)$$

From equation (40):

$$\frac{\partial \phi}{\partial c} = V \left[\frac{2c}{r} \right] \cos \theta = \frac{\partial \phi}{\partial R}, \text{ since } c = R \text{ in case 3.}$$

Also, from Figure 2:

$$\frac{dR}{dx} = \tan \beta \text{ (a negative quantity),}$$

And, by definition:

$$\frac{dx}{dt} = -U = -U_0 \cos \alpha = \text{the stream velocity parallel to the x-axis.}$$

Putting all of this information into equation (48), we get:

$$\begin{aligned}
\frac{\partial \phi}{\partial t} &= V \left[\frac{2c}{r} \right] (\cos \theta) (-\tan \beta) (-U_o \cos \alpha) \\
&= U_o \sin \alpha \left(\frac{2c}{r} \right) \cos \theta \tan \beta U_o \cos \alpha \\
&= U_o^2 \left(\frac{R}{r} \right) \cos \theta \tan \beta \sin 2\alpha \quad (49)
\end{aligned}$$

Note in equation (49) that two negative quantities exist, but their sign is inherent, so that we need concern ourselves only with their absolute values. That is, the complex potential ϕ defined by equation (40) is for a stream moving with velocity V in the negative-y direction, and the fact that $R(x)$ decreases with x has been accounted for in the first step above by putting a minus sign in front of $\tan \beta$. Should the circumstances of Figure 2 change from those indicated, care must be taken to make the appropriate sign changes where necessary. Essentially, equation (49) postulates an analogy between the variation of cross-flow with x on a truncated cone configuration, and the variation of cross-flow with t on a circular cylinder configuration started impulsively from rest in a stationary, unbounded fluid (for further discussion of this point, see Allen and Perkins, 1951).

Now, if we let $V = U_o \sin \alpha$ in equation (47) and substitute (47) and (49) into (42), we get:

$$\begin{aligned}
\frac{1}{2} U_o^2 \sin^2 \alpha \left[\left(1 - \frac{R^2}{r^2} \right)^2 \cos^2 \theta + \left(1 + \frac{R^2}{r^2} \right)^2 \sin^2 \theta \right] \\
- U_o^2 \left(\frac{R}{r} \right) \cos \theta \tan \beta \sin 2\alpha + \frac{p}{\rho} = C_o \quad (50)
\end{aligned}$$

As $r \rightarrow \infty$, p approaches some free stream pressure, p_o , so that:

$$C_o = \frac{p_o}{\rho} + \frac{1}{2} U_o^2 \sin^2 \alpha \quad (51)$$

Equation (50), with C_o defined by equation (51) can be used to calculate the pressure, p anywhere in the flow field. We are most interested, however, in what happens on the surface of the cone. Thus, let $r = R$ to get:

$$\frac{1}{2} U_o^2 \sin^2 \alpha (4 \sin^2 \theta) - U_o^2 \cos \theta \tan \beta \sin 2\alpha + \frac{p}{\rho} = \frac{p_o}{\rho} + \frac{1}{2} U_o^2 \sin^2 \alpha \quad (52)$$

At this point, it is convenient to define a dimensionless surface pressure coefficient, $C_p = \frac{p - p_o}{\frac{1}{2} \rho U_o^2}$. Then, from equation (52):

$$C_p = \sin^2 \alpha [1 - 4 \sin^2 \theta] + 2 \cos \theta \tan \beta \sin 2\alpha \quad (53)$$

Note, in equation (53) that $C_p = 0$ (i.e., $p = p_o$) if $\alpha = 0^\circ$, that is, if the stream approaches the limb parallel to its centerline, the x-axis. In fact, this is strictly true only if $\beta = 0^\circ$ as well, i.e., if the limb configuration is a perfect right circular cylinder. If $\beta \neq 0$, such that the limb configuration is that of a truncated cone facing a stream coming along parallel to the x-axis, then the surface pressure at any station, designated $p_{\alpha=0}$, will differ slightly from the static pressure, p_o , for small β .

The discrepancy in equation (53) stems from the fact that the derivation of this equation for C_p has concerned itself only with the effects due to a cross-flow, V , coming at the limb. Account has not been taken of the pressure distribution generated on the inclined conical surface as a result of the axial-flow component, U . In the work of Allen and Perkins (1951), an argument is presented for considering that this latter pressure distribution remains constant with α , adds linearly to C_p for small β and reduces to zero for $\beta = 0$. Thus, we may simply add an arbitrary correction factor to equation (53), in the form of a pressure coefficient designating the effects on the surface due to U :

$$C_p = \sin^2 \alpha [1 - 4 \sin^2 \theta] + 2 \cos \theta \tan \beta \sin 2\alpha + C_{p_{\alpha=0}} \quad (54)$$

where it is assumed that $C_{p_{\alpha=0}}$ does not vary much with α (for small β) and goes to zero with β . For the time being, this latter pressure coefficient needs to be determined empirically, and we shall neglect it temporarily. In fact, it turns out that the contribution of $C_{p_{\alpha=0}}$ to total cross-force calculations is not important because its integral around the surface vanishes in this direction (Allen and Perkins, 1951).

Note further, that, when $\beta = 0$ [$C_{p_{\alpha=0}} = 0$, $\tan \beta = 0$] and $\alpha = 90^\circ$ ($\sin^2 \alpha = 1$, $\sin 2\alpha = 0$) equation (54) reduces to the classical equation for the pressure distribution on a right circular cylinder oriented with its axis normal to a stream coming at it with velocity V ($\tan \alpha = \frac{V}{U} = \infty$, $U = 0$):

$$C_p = 1 - 4 \sin^2 \theta \quad (55)$$

For the problem under consideration, large values of α are not unlikely because the presence of a torso (Figure 3) deflecting an oncoming stream of fluid would cause that fluid to approach the forearm at a rather large angle of attack.

Equation (53) is shown plotted in Figures 6 and 7 for two values of β , with α acting as a parameter. These two figures, together with equations (47), (52) and (53) may be used to illustrate several important points. First, we observe in equation (47) that stagnation points ($q = 0$) exist on the surface ($r = c = R$) of the limb at $\theta = 0^\circ$ and 180° . The stagnation point at 0° is undoubtedly correct, whereas the one at 180° must be viewed more carefully in terms of the separated flow patterns on the lee side of bluff bodies. For $\theta = 0^\circ$, equation (53) becomes:

$$C_p = \sin^2 \alpha + 2 \tan \beta \sin 2\alpha \quad (56)$$

and we see that $C_p = 1$ for $\alpha = 90^\circ$ ($p = p_o + \frac{1}{2} \rho U_o^2 = \text{maximum}$), $C_p = 0$ for $\alpha = 0^\circ$ ($p = p_o$). Thus, $0 \leq C_p \leq 1$ for $0^\circ \leq \alpha \leq 90^\circ$ with $\theta = 0^\circ$ (or 180°), which is shown clearly in Figures 6 and 7.

Second, if we differentiate equation (52) with respect to θ and set the result equal to zero, this yields:

$$\frac{\partial p}{\partial \theta} = \rho \left[\frac{1}{2} U_o^2 \sin^2 \alpha (8 \sin \theta \cos \theta) (-1) + U_o^2 (-\sin \theta) \tan \beta \sin 2\alpha \right] = 0 \quad (57)$$

from which:

$$\cos \theta = - \frac{\tan \beta}{\tan \alpha} \frac{1}{2} \quad (58)$$

Observe, then, that, for β finite (not equal to zero), $\cos \theta$ varies as the inverse of $\tan \alpha$. Substituting equation (58) into (53) gives:

$$\begin{aligned} C_p &= \sin^2 \alpha \left[1 - 4 \left(1 - \frac{1}{4} \frac{\tan^2 \beta}{\tan^2 \alpha} \right) \right] + 2 \left[- \frac{1}{2} \frac{\tan \beta}{\tan \alpha} \right] \tan \beta \sin 2\alpha \\ &= \sin^2 \alpha \left[1 + \tan^2 \beta \frac{\cos^2 \alpha}{\sin^2 \alpha} - 4 \right] - \tan^2 \beta (2 \sin \alpha \cos \alpha) \frac{\cos \alpha}{\sin \alpha} \end{aligned}$$

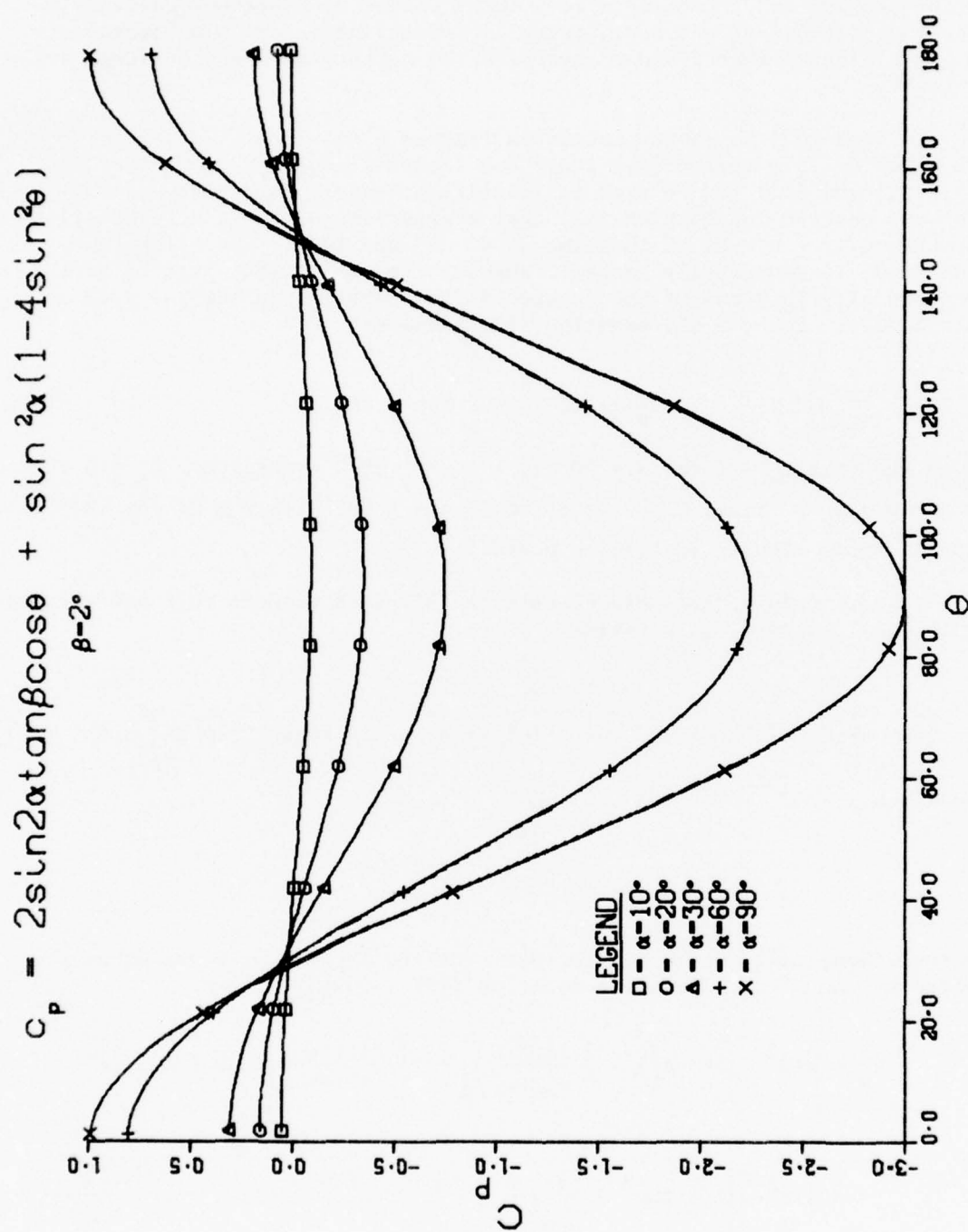


Figure 6. Surface pressure distribution around forearm having two degree angle of taper and sitting free (i.e., not in contact with any surface) in wind stream.

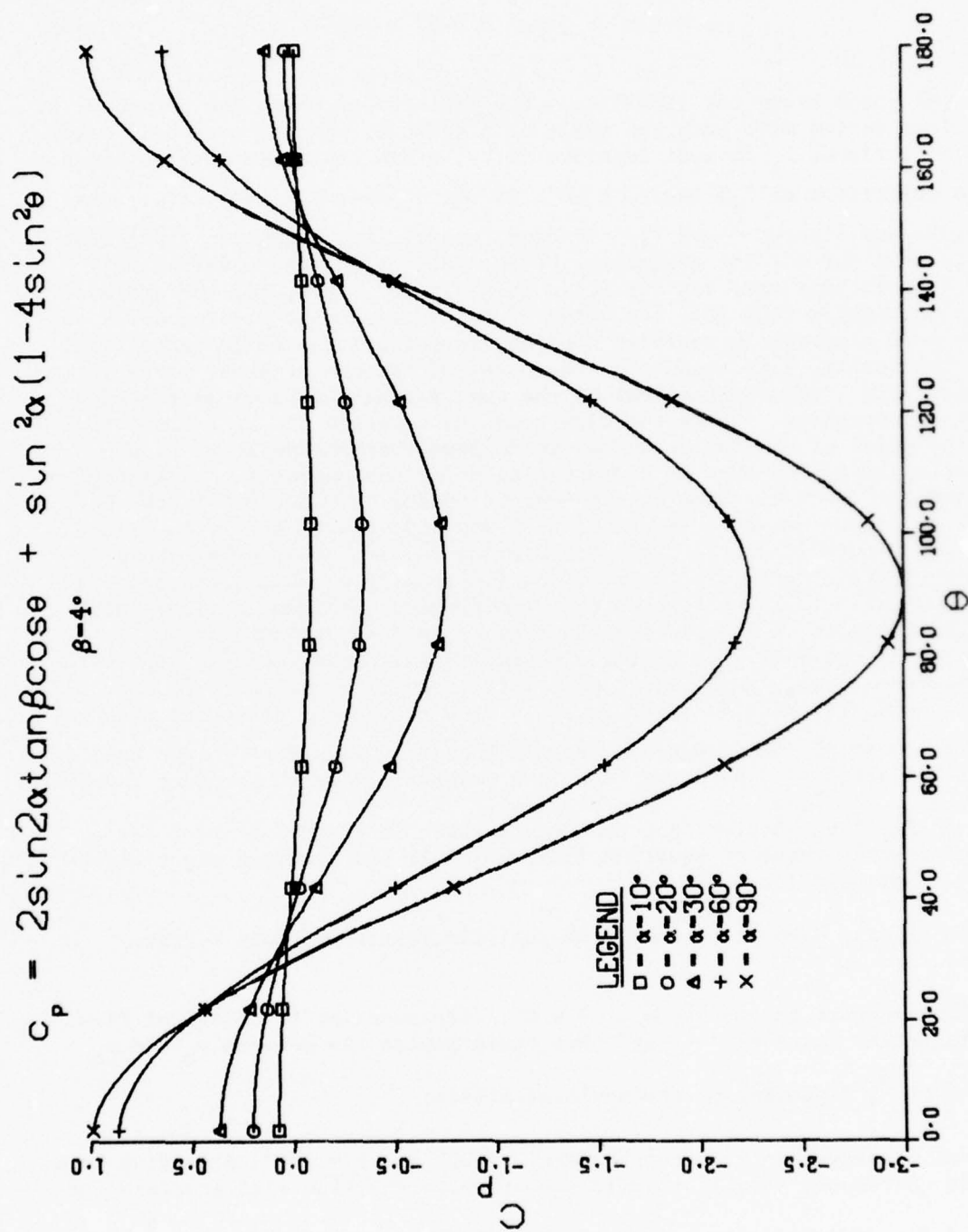


Figure 7. Surface pressure distribution around forearm having four degree angle of taper and sitting free in wind stream.

$$\begin{aligned}
C_p &= -3 \sin^2 \alpha - \cos^2 \alpha \tan^2 \beta \\
&= \sin^2 \alpha [\tan^2 \beta - 3] - \tan^2 \beta
\end{aligned} \tag{59}$$

Thus, the point along the limb (i.e., the angle θ) at which the pressure, p , is minimum varies with both the angle of attack, α , and the cone half-angle, β . With β fixed, C_p is most negative (i.e., p has its minimum value based on the definition of C_p) when $\alpha = 90^\circ$, at which point $C_p = -3$ (c.f., equation (59) and Figures 6 and 7). In fact, we see (from equation (59)) that this is true for $\alpha = 90^\circ$ regardless of the value of β , and equation (58) shows that in this case $\cos \theta = 0$, so that $\theta = 90^\circ$. Now, for the angle of attack decreasing from 90° , the value of $\tan \alpha$ decreases, causing $\cos \theta$ to become more negative in equation (58) and thus forcing θ to increase from 90° . Physically, this means that the point of minimum pressure moves more lee-ward (i.e., towards the rear of the cone facing the flow) as the angle of attack decreases. Since the flow tends to separate off of a bluff body near the point of minimum pressure, it follows that the point of flow separation moves lee-ward with decreasing α for the geometric configuration depicted in Figure 2. Such motion depends weakly on the angle β (for β small) in accordance with equations (58) and (59) above, and it is illustrated in Figures 6 and 7. Here the minimum value of the curves shown is seen to be drifting slowly to the right (increasing θ) as α decreases from 90° . Note also in these figures that the pressure minimum increases with decreasing angles of attack, such that there is less pressure to be recovered on the back side of the limb as its axis comes more in line with the incident flow. In the limit of $\alpha \rightarrow 0$, there is no pressure loss at all as the fluid traverses θ . That is, $C_p = 0$ as previously discussed with respect to equation (53). However, recall that this is strictly true only if we can neglect $C_{p_{\alpha=0}}$, which we have done temporarily in the present investigation. Finally, observe that the curves shown in Figures 6 and 7 for $\alpha = 90^\circ$ are exactly those of equation (55), which is the standard right-circular-cylinder solution.

To briefly summarize, then, the analytic results of this section reveal:

- 1) that pressure maxima occur at $\theta = 0^\circ$, corresponding to points of flow stagnation for $\alpha \neq 0^\circ$ -- and that these maxima lie between p_0 and $p_0 + \frac{1}{2} \rho U_0^2$, depending on the angle of attack;
- 2) that pressure minima occur between $\theta = 90^\circ$ and $\theta = 180^\circ$, depending on α , and correspond roughly to points near where the flow will separate for $\alpha \neq 0^\circ$. The pressure at these points lies between p_0 and $p_0 - \frac{3}{2} \rho U_0^2$,

and the points themselves move leeward (increasing θ) with decreasing α at a rate mildly dependent on β (for β small).

The Special Case $n = 0$

We move on, now, to examine the case of the forearm resting, but not pressing against an arm rest (case 2, Figure 3, $n = 0$). Thus, consider the complex velocity potential given by equation (33), together with its complex conjugate, $\bar{w} = \pi a V \coth \frac{a\pi}{\chi}$. From equation (27), we have:

$$q^2 = \frac{dw}{d\chi} \frac{d\bar{w}}{d\chi} = \frac{a^4 \pi^4 V^2}{\chi^2 \chi^2} \operatorname{cosech}^2 \frac{a\pi}{\chi} \operatorname{cosech}^2 \frac{a\pi}{\chi} \quad (60)$$

which, upon expanding in accordance with the definition of χ , $\bar{\chi}$, and performing some algebraic simplifications, becomes:

$$q^2 = \frac{a^4 \pi^4 V^2}{r^4} \left[\frac{2}{\cosh \frac{2a\pi y}{r^2} - \cos \frac{2a\pi z}{r^2}} \right]^2 \quad (61)$$

where: $r^2 = y^2 + z^2$. On the surface of the limb, $r^2 = 2az$ (from equations (15) and (32)), so that equation (61) becomes:

$$q^2 = \frac{a^2 \pi^4 V^2}{4z^2} \operatorname{sech}^4 \frac{\pi y}{2z} \quad (62)$$

Similarly, on the plane to which the cone is tangent, $z = 0$, so that equation (61) reduces to:

$$q^2 = \frac{a^4 \pi^4 V^2}{y^4} \operatorname{cosech}^4 \frac{a\pi}{y} \quad (63)$$

For the case $n = 0$, equation (45) becomes,

$$\frac{\partial \phi}{\partial t} = \frac{\partial \phi}{\partial a} \frac{\partial a}{\partial t} = \frac{\partial \phi}{\partial a} \frac{da}{dx} \frac{dx}{dt} \quad (64)$$

where ϕ is given by equation (34) and "a" is the radius of the forearm (equation (32)), which varies from the wrist to the elbow (along x) as shown in Figure 3. From equation (34):

$$\frac{\partial \phi}{\partial a} = \frac{\pi V \sec^2 \frac{a\pi z}{r^2}}{\left\{ \tanh^2 \frac{a\pi y}{r^2} + \tanh^2 \frac{a\pi z}{r^2} \right\}^2} \left\{ \left[\tanh \frac{a\pi y}{r^2} \sec^2 \frac{a\pi z}{r^2} \right] - \left(\operatorname{sech}^2 \frac{a\pi y}{r^2} \right) \left[\tanh \frac{a\pi y}{r^2} \left(1 + \frac{2a\pi z}{r^2} \tanh \frac{a\pi z}{r^2} \right) + \frac{a\pi y}{r^2} \left(\tanh^2 \frac{a\pi y}{r^2} - \tanh^2 \frac{a\pi z}{r^2} \right) \right] \right\} \quad (65)$$

Again, we may write:

$$\frac{da}{dx} = \tan \beta \text{ (a negative quantity)}, \quad (66)$$

and,

$$\frac{dx}{dt} = -U_o \cos \alpha. \quad (67)$$

To simplify the mathematics, recall that we are most interested in what happens on the surface of the limb. Thus, substituting $r^2 = 2az$ into equation (65) and putting that, together with the expressions (66) and (67) into (64), yields:

$$\frac{\partial \phi}{\partial t} = \pi(U_o \sin \alpha) \left[\tanh \frac{\pi y}{2z} + \frac{\pi y}{2z} \operatorname{sech}^2 \frac{\pi y}{2z} \right] (-\tan \beta) (-U_o \cos \alpha) \quad (68)$$

We comment here that equation (65) needs to be multiplied by $\cos^4 \frac{a\pi z}{r^2}$ on top and bottom in order that its limit as $r^2 \rightarrow 2az$ may be determined. Furthermore, a negative sign has again been inserted before the $\frac{da}{dx}$ term in equation (68) in order to account for the fact that $\tan \beta$ is a negative quantity as discussed previously. Finally, it is a relatively straightforward matter to show that the limit of equation (65) as $r \rightarrow \infty$ is zero, and that of equation (61) is V^2 . Thus, from Bernoulli's equation applied at infinity, we again arrive at the conclusion that:

$$C_o = \frac{p_o}{\rho} + \frac{1}{2} U_o^2 \sin^2 \alpha \quad (69)$$

and therefore, equation (42), written for the surface of the forearm using equations (62), (68) and (69), becomes:

$$\frac{a^2 \pi^4 U_o^2 \sin^2 \alpha}{8z^2} \operatorname{sech}^4 \frac{\pi y}{2z} - \frac{\pi}{2} (\sin 2\alpha) U_o^2 \left[\tanh \frac{\pi y}{2z} + \frac{\pi y}{2z} \operatorname{sech}^2 \frac{\pi y}{2z} \right] (\tan \beta) \\ + \frac{p}{\rho} = \frac{p_o}{\rho} + \frac{1}{2} U_o^2 \sin^2 \alpha \quad (70)$$

or, in the form of the non-dimensionalized surface pressure coefficient,

$$C_p = \frac{p - p_o}{\frac{1}{2} \rho U_o^2} = \sin^2 \alpha \left[1 - \frac{a^2 \pi^4}{4z^2} \operatorname{sech}^4 \frac{\pi y}{2z} \right] + \pi \sin 2\alpha \tan \beta \left[\tanh \frac{\pi y}{2z} \right. \\ \left. + \frac{\pi y}{2z} \operatorname{sech}^2 \frac{\pi y}{2z} \right] \quad (71)$$

where $\frac{y}{z} = \cot \theta$ (see Figure 4), $r^2 = 2az$ and we are still neglecting the contribution from the axial flow component, U , in the form of $C_{p_{\alpha=0}}$ as we did before. That is, note again in equation (71) that $C_p = 0$, i.e., $p = p_o$ when $\alpha = 0^\circ$. Now, from Figure 4, it is possible to write:

$$\sin^2 \theta = \frac{z^2}{r^2} = \frac{z^2}{2az} = \frac{z}{2a}, \text{ so that: } z^2 = 4a^2 \sin^4 \theta \quad (72)$$

Substituting equation (72) into equation (71), we may write:

$$C_p = \sin^2 \alpha \left[1 - \frac{\pi^4 \operatorname{sech}^4 \left(\frac{\pi}{2} \cot \theta \right)}{16 \sin^4 \theta} \right] + \pi \sin 2\alpha \tan \beta \left[\tanh \left(\frac{\pi}{2} \cot \theta \right) \right. \\ \left. + \frac{\pi}{2} \cot \theta \operatorname{sech}^2 \left(\frac{\pi}{2} \cot \theta \right) \right] \quad (73)$$

which is an expression analogous to equation (53), giving C_p as a function of α , β , and θ .

When $\beta = 0^\circ$ $\left[C_{p_{\alpha=0}} = 0, \tan \beta = 0 \right]$ and $\alpha = 90^\circ$ ($\sin^2 \alpha = 1, \sin 2\alpha = 0$) equation (73) reduces to:

$$C_p = 1 - \frac{\pi^4 \operatorname{sech}^4\left(\frac{\pi}{2} \cot \theta\right)}{16 \sin^4 \theta} \quad (74)$$

which is the equivalent of equation (55) written for a free right circular cylinder. It is interesting to compare the results obtained from equations (55) and (74). For example, at the top of the cylinder $\left(\theta = \frac{\pi}{2}\right)$ equation (55) gives $C_p = -3$, whereas equation (74) yields $C_p = -5$. Thus, the pres-

sure coefficient in the latter case is some 67% lower than it is for the free cylinder, indicating that the presence of the flat surface causes the pressure at the top of the cylinder to be greatly reduced compared with the corresponding case where the surface of contact is absent. Moreover, for θ

small, $\cot \theta \approx \frac{1}{\theta}$, $\operatorname{sech}^4\left(\frac{\pi}{2\theta}\right) \approx 16e^{-\frac{2\pi}{\theta}}$, and $\sin^4 \theta \approx \theta^4$, so that equation (74) becomes:

$$C_p \approx 1 - \left(\frac{\pi^2 e^{-\frac{\pi}{\theta}}}{\theta^2} \right)^2 \quad (75)$$

the limit of which, as $\theta \rightarrow 0$ is 1. At the bottom of the cylinder, where it is in contact with the flat surface, we therefore have a stagnation point ($q = 0$) at which $C_p = 1$ for $\alpha = 90^\circ$. The pressure at this point is much higher than it is at the bottom of a cylinder sitting free in an unbounded flow, where equation (55) reveals that $C_p = -3$ when $\theta = -\frac{\pi}{2}$. The effect of the flat surface, then, is to distort the symmetric pressure distribution around the cylinder, such that the pressure is higher at the bottom ($\theta = 0^\circ$ in Figure 4) than it is at the top ($\theta = 90^\circ$). In fact, it is higher by an amount:

$$(C_p)_{\theta=0} - (C_p)_{\theta=90} = \frac{p_{\text{bottom}} - p_{\text{top}}}{\frac{1}{2} \rho U_o^2} = 1 - \left[1 - \frac{\pi^4}{16} \right],$$

$$\Delta p = p_{\text{bottom}} - p_{\text{top}} = \frac{\rho U_o^2 \pi^4}{32} \quad (76)$$

There is thus a tendency for the cylinder to be lifted from the surface by a maximum pressure gradient of some six times the free stream dynamic pressure, $\frac{1}{2} \rho U_o^2$.

At the stagnation point $\theta = 0$, where the static pressure has its maximum value on the surface of the conical limb, equation (73) reduces to:

$$C_p = \sin^2 \alpha + \pi \sin 2\alpha \tan \beta \quad (77)$$

which is similar to equation (56), differing only in the coefficient of the second term on the right hand side. The first term follows directly from the discussion which has preceded equation (75). The second term results from the fact that, for θ small, $\tanh\left(\frac{\pi}{2}\cot\theta\right)\theta + \frac{\pi}{2}\cot\theta \operatorname{sech}^2\left(\frac{\pi}{2}\cot\theta\right) \approx$

$$\tanh\left(\frac{\pi}{2\theta}\right) + \frac{\pi}{2\theta}\operatorname{sech}^2\left(\frac{\pi}{2\theta}\right) \approx 1 + \frac{\pi}{2\theta} 4e^{-\frac{\pi}{\theta}}, \text{ the limit of which is 1 as } \theta \rightarrow 0.$$

Thus, again we see that $C_p = 1$ for $\alpha = 90^\circ$ ($p = p_o + \frac{1}{2}\rho U_o^2 = \text{maximum}$), $C_p = 0$ for $\alpha = 0^\circ$ ($p = p_o$), and $0 \leq C_p \leq 1$ for $0^\circ \leq \alpha \leq 90^\circ$. The difference between this case and the previous section, however, is that equation (77) holds at the bottom of the forearm, whereas equation (56) holds at the forward stagnation point along the front side of the limb.

At the top of the cone equation (73) becomes (for $\theta = 90^\circ$):

$$C_p = \sin^2 \alpha \left[1 - \frac{\pi^4}{16} \right] \quad (78)$$

so that:

$$(C_p)_{\theta=0} - (C_p)_{\theta=90} = \frac{p_{\text{bottom}} - p_{\text{top}}}{\frac{1}{2}\rho U_o^2} = \pi \sin 2\alpha \tan \beta + \frac{\pi^4}{16} \quad (79)$$

The pressure gradient tending to "lift" the forearm off of the seat arm rest thus appears to increase with α up to a maximum for $\alpha = 45^\circ$. However, the variation of Δp with α is scaled by $\tan \beta$, which is very small in the physiologic range. For β as high as 10° , for example, the maximum value of

$\pi \sin 2\alpha \tan \beta$ is only 0.55, compared with the value of $\frac{\pi^4}{16}$ which is 6.09.

This may, or may not be significant for very large values of U_o , and viewed in terms of the ability of the forearm musculature to resist displacing forces, it could turn out to be critical. In any event, the tendency for limb-displacement seems to be substantial in cases where the interaction of the limb with a solid surface produces a stagnation point in the flow -- especially if the flow is high-speed.

If we differentiate equation (73) with respect to θ and set the result equal to zero, this is equivalent to finding the point along the surface where the pressure as defined by equation (70) is a minimum. Letting

$\delta = \frac{\pi}{2} \cot \theta$, it is found, after some algebra, that θ must satisfy the

relation:

$$\frac{\sin 2\theta - \pi \tanh \delta \operatorname{sech}^2 \delta}{\sin 2\theta \tanh \delta + 2 \frac{\operatorname{sech}^2 \delta}{\sin^4 \theta}} = \frac{8 \tan \beta}{\pi^2 \tan \alpha} \quad (80)$$

which is analagous to equation (58) for the case of the free cone. Thus, again we find that the angle for which the pressure is minimum varies with both α and β , with $\alpha = 90^\circ$ causing C_p to have its minimum value (just under -5) at $\theta = 90^\circ$ -- the very top of the limb. This is clearly illustrated in Figures 8 and 9, where equation (73) is plotted for two values of β , with α acting as a parameter. Comparison of these two Figures with Figures 6 and 7 reveals a qualitative similarity in the general character of the curves shown, but also highlights some dramatic differences. For example, note how flat the curves of Figures 8 and 9 are for θ between 0° and 40° , and again between 140° and 180° . This represents a very high pressure region ($C_p > 0$) spanning some 160° of arc along the lower half of the circular cross section in contact with the flat surface (note that an inscribed angle has the same measure, in angle degrees, as half of its intercepted arc, in arc degrees). For θ between 40° and 140° the pressure drops off quite sharply, and there results a significant low pressure region for the remaining 200° of arc. Thus, Figures 8 and 9 reinforce the concept that large forces exist which tend to dislodge a limb from a surface with which it is in contact. In the present context, such forces arise as a result of causing a high-speed flow to stagnate. Later on, we shall discuss (in principle, for the moment) additional forces that arise as a result of causing a flowing stream of fluid to separate from (or to fail to follow the contour of) a solid surface with which it is in contact. Note further in Figures 8 and 9 that the minima of the curves shown also drift to the right (increasing θ) with decreasing angle of attack, and that their magnitude increases. As was the case for the free cone, this means that the point of minimum pressure moves lee-ward as the angle of attack decreases (as does the corresponding point of flow separation) and there is also less pressure to be recovered on the back side of the limb as its axis comes more in line with the incident flow. These events are dependent on the angle β in accordance with equation (80).

Summarizing, then, the essential analytic findings of this section, we see:

- 1) that pressure maxima occur at the point of contact between a conical surface and a flat restraining plate, varying in magnitude from p_0 at $\alpha = 0^\circ$ to $p_0 + \frac{1}{2} \rho U_0^2$ at $\alpha = 90^\circ$ and caused by stagnation of the flow at this point;
- 2) that there is a high pressure region spanning nearly 160° of arc along the lower half of the circular cross section in contact with a flat surface;
- 3) that there is a relatively deep low pressure region spanning nearly 200° of arc along the top of the forearm, such that there results a rather

$$C_p = \sin^2 \alpha \left\{ 1 - \left[\frac{\pi \operatorname{sech} \delta}{2 \sin \theta} \right]^4 \right\} + \pi \sin 2\alpha \tan \beta (\tanh \delta + \delta \operatorname{sech} \delta)$$

where $\delta = \frac{\pi \cot \theta}{2}$

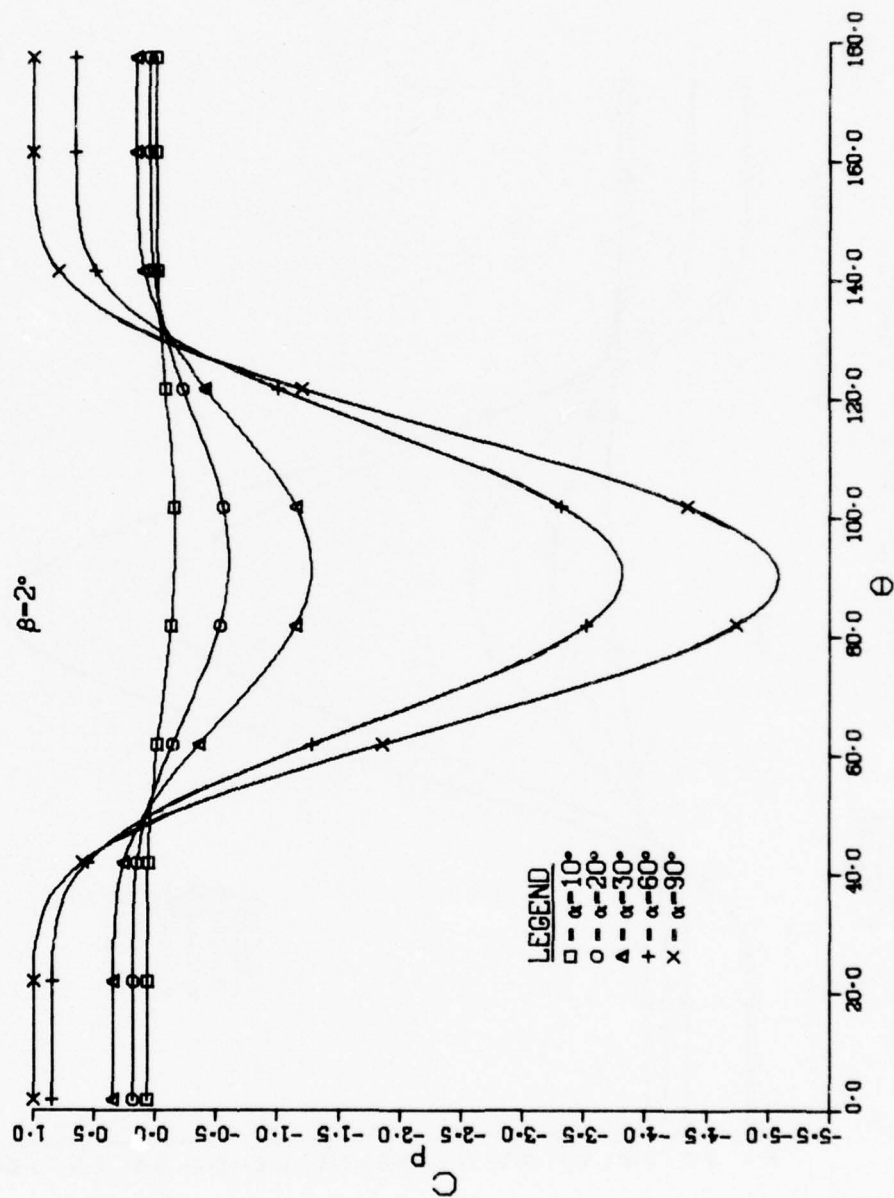


Figure 8. Surface pressure distribution around forearm having two degree angle of taper and resting, but not pressing against an arm rest.

$$C_p = \sin^2 \alpha \left\{ 1 - \left[\frac{\pi \operatorname{sech} \delta}{2 \sin \theta} \right]^4 \right\} + \pi \sin 2\alpha \tan \beta (\tanh \delta + \delta \operatorname{sech}^2 \delta)$$

where $\delta = \frac{\pi \cot \theta}{2}$

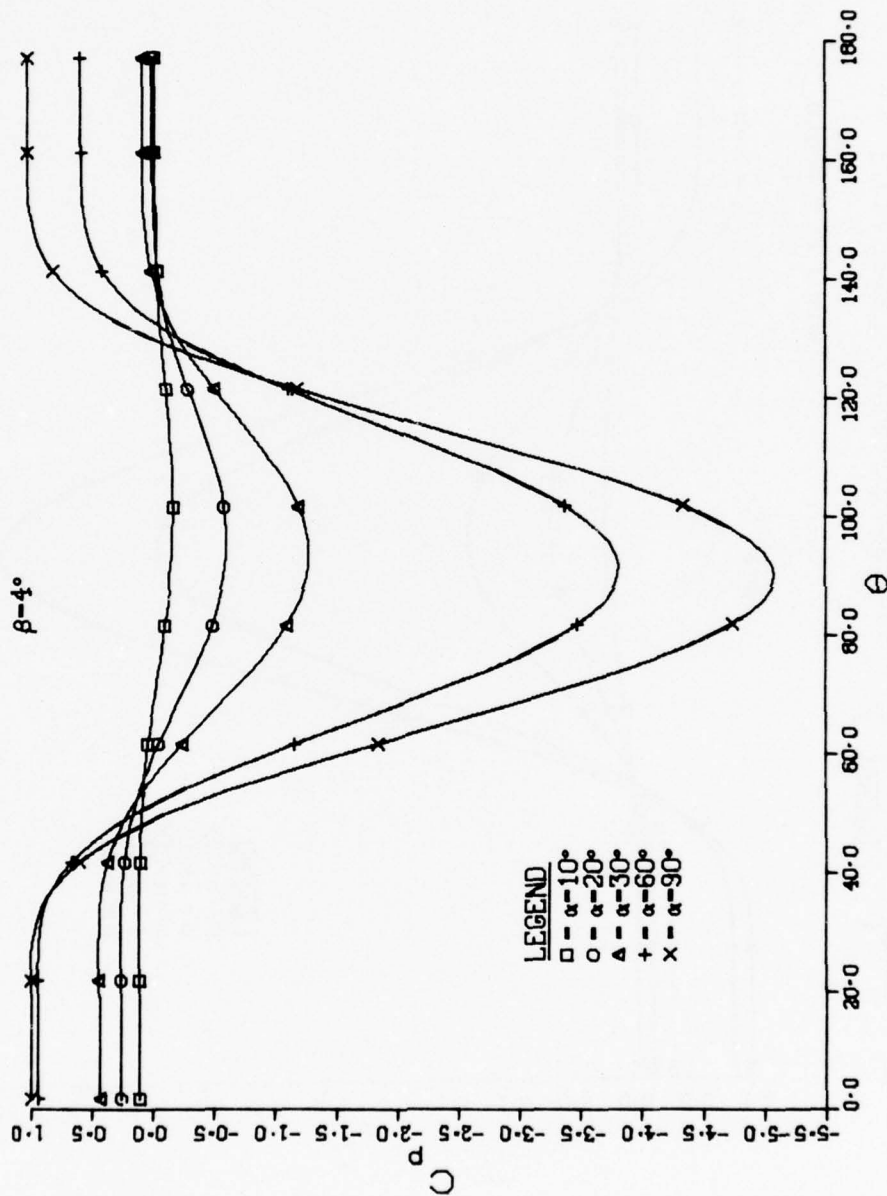


Figure 9. Surface pressure distribution around forearm having four degree angle of taper and resting, but not pressing against an arm rest.

substantial net force that acts to lift the cone (or dislodge the limb) from the surface with which it is in contact;

- 4) that pressure minima occur near the top of the limb and move lee-ward with decreasing angle of attack at a rate mildly dependent on the cone half-angle. These pressure minima correspond roughly to points near where the flow will separate, and their value lies between p_o and $p_o - \frac{5}{2} \rho U_o^2$, depending on α .

SECTION VII

THE EFFECTS OF FLUID VISCOSITY

The significance of fluid viscosity in the real world can be dramatically illustrated by a simple calculation. Let us consider, for example, the total cross-force per unit length of cone predicted by the inviscid theory of Section VI, in the special case $n = 1$. For this case, the cross-force per unit length may be written:

$$f = \int_0^{2\pi} (p_{\text{surface}}) \cos \theta R d\theta \quad (81)$$

where p_{surface} is defined by equations (52) and, more generally, (54), i.e.,

$$p_{\text{surface}} = p_o + C_p \left[\frac{1}{2} \rho U_o^2 \right] \quad (82)$$

$$C_p = \sin^2 \alpha \left[1 - 4 \sin^2 \theta \right] + 2 \cos \theta \tan \beta \sin 2\alpha + C_{p_{\alpha=0}} \quad (83)$$

Substituting equations (82) and (83) into (81) and performing the indicated integration leads to the result:

$$f = \pi \rho U_o^2 R \sin 2\alpha \tan \beta \quad (84)$$

which is a force acting in the x-y plane, located midway between the normal to the axis of revolution of the cone and the normal to the wind direction (see Allen and Perkins, 1951). Examining equation (84) more closely, one sees that the inviscid theory predicts that $f = 0$, i.e., there is no net cross-force acting on the limb when $\beta = 0^\circ$ (that is, if the truncated cone reduces to a simply right-circular cylinder) or when $\alpha = 90^\circ$ (that is, if the truncated cone has its axis at right angles to the incident stream). Clearly, this result is nonsense, for it says, in effect, that there is no such thing as drag. This type of reasoning, together with some simple experimental observations, is what led Prandtl, at the turn of the century,

to formulate his classic theory of the boundary layer. Essentially, Prandtl argued that no matter how small the viscosity of a fluid was, and no matter how high the Reynolds number of the flow was, the effect of fluid viscosity could not be neglected--that is, the flow could not be considered to be inviscid in the immediate vicinity of a bounding surface. Physically, this is due to the nature of frictional interactions which take place between fluid and surface, leading to significant losses of kinetic energy. The lost energy becomes critical if the fluid flows against an adverse pressure gradient, i.e., if the pressure increases in the direction of flow, as it does on the lee side of blunt bodies (see Figures 6, 7, 8 and 9 for $\theta > 90^\circ$). In such cases, the fluid nearest to the surface may have insufficient energy to travel "uphill" and it therefore either comes to rest or reverses its direction of motion under the influence of the adverse pressure gradient. When this happens, the fluid still moving downstream loses contact with the bounding surface and we say that the flow has "separated", or failed to follow faithfully the contour of the boundary to which it was originally attached.

The phenomenon of flow separation is the most important aspect of high-speed flow over blunt bodies of revolution. Unfortunately, it is also the most difficult to handle analytically because of the nonlinear elliptic nature of the problem. Thus, much of the work in this area during the pre-large-high-speed-computer years was experimental, and the theories formulated were semi-empirical. For instance, to correct equation (84) for the observed effects of fluid viscosity, an additional term was simply added linearly to the potential flow solution. This term included an experimentally determined "drag coefficient", defined as:

$$C_D = \frac{\text{"viscous" drag force per unit length of surface}}{\frac{1}{2} \rho V^2} \quad \text{per unit of projected area normal to the flow.} \quad (85)$$

In equation (85), the "viscous" drag actually includes two effects -- one is due to the rubbing or shearing action attributable to friction between surface and fluid; the other is due to separation of the flow itself, which results in what is called a profile, or form drag. Profile drag is not a shearing action. It is a net drag force which results from a high-pressure area on the windward side of a bluff body and a low-pressure area on the lee side, the latter being a direct consequence of flow separation. In other words, the high energy losses associated with separation of the flow do not allow for the complete pressure recovery shown ideally in Figures 6 through 9 by the symmetry of the curves with respect to their respective minimum value. Instead, there is a significant loss of pressure energy on the back side of a blunt body, such that the pressure distribution in the separated region of flow no longer balances that on the front side of the body, and there is a net pressure drag due to viscosity. In the problem being considered here, profile, or form drag is by far the dominant factor in equation (85). This was discussed earlier in Section III (Preliminary Assumptions) and is important in that it allows C_D to be handled analytically as described later.

Recalling that $V = U_o \sin \alpha$, and noting that the projected area normal to the flow per unit length of a cone of radius $R(x)$ is, locally, $2R(x)$, we may write the viscous drag force in equation (85) as:

$$f_D(x) = \rho U_o^2 R(x) C_D(x) \sin^2 \alpha \quad \begin{array}{l} \text{per unit length} \\ \text{of surface,} \end{array} \quad (86)$$

where $C_D(x)$ is the "local" drag coefficient at station x , meaning that it is a function of $R(x)$, as well as the local mean Reynolds number, $\rho VR(x)/\mu$, and the Mach number, V/V^* . V^* represents the local speed of sound and μ is the viscosity of the fluid. Observe that this force is in the direction of V , such that the tendency is for the flow to pull the blunt object along with it. Bearing in mind the discussion of Section VI relative to an object in contact with a flat solid surface (where it was shown that there is a net force tending to lift the object from the surface), we may now conclude that the forearm in contact with a seat arm rest is subjected to forces which tend to pull it up (away from its support) and out (away from the thorax) due, respectively to the generation of lift and drag forces in the configuration described. This result is in agreement with wind tunnel experiments, which have shown a distinct upward and outward motion of the forearm when subjected to conditions similar to those simulated here (Brinkley, J. W., personal communication, and 1974 reference).

The Determination of C_D

In general, the drag coefficient is an experimentally determined quantity. Allen and Perkins (1951) suggest a means for estimating this quantity for a slender body with varying cross-sectional area. They first define an

effective diameter, $D' = \frac{A_p}{L}$, where A_p , the plan-form area is given by

$$2 \int_0^L R(x) dx, \text{ and } L \text{ is the total length of the body. Then, they obtain a}$$

tabulated drag coefficient C_D for a circular cylinder of diameter D' at the

cross-flow Reynolds Number, $\frac{U_o \sin \alpha (\rho D')}{\mu}$, and the cross-flow Mach Number,

$\frac{U_o \sin \alpha}{V^*}$. Finally, they correct C_D for the effect of the finite fineness

ratio, $\frac{L}{D'}$, as discussed (and for which tabulated data is presented) by

Goldstein (1938, pp. 418-421, and 439) and assume that the slender body behaves with essentially the same characteristics as this fictitious circular cylinder of constant diameter D' .

Kelly (1954) refined the approach of Allen and Perkins to include transient effects related to flow development over the blunt body. He defines a dimensionless parameter, $\frac{V}{R} t = \frac{U_o \sin \alpha}{R} \frac{x}{U_o \cos \alpha} = \frac{x}{R} \tan \alpha$, such that:

$$C_D = \sum_{m=0}^{m=\infty} C_m \frac{x^{2m+1}}{R^{2m+1}} \tan^{2m+1} \alpha \quad (87)$$

where the various C_m are still experimentally evaluated coefficients.

In 1959, Mello (1959) pointed out that the results of Allen, Perkins and Kelly were all strongly dependent on the body fineness ratio and the angle of attack, due to their basic inability to adequately predict the magnitude and distribution of forces resulting from flow separation. Following reasoning similar to that employed in justifying assumption 2 of section III, Mello therefore proposed to model theoretically the separated flow regime on the leeward side of bodies of revolution. His model consisted of simple line vortices symmetrically situated (along the z-axis of Figure 2) on the lee side of a circular cylinder in a uniform stream, and he utilized potential flow theory to define mathematically the corresponding flow field. Mello was then able to show that a simple relationship existed between the strength of the vortices and the viscous normal force acting on the cylinder, i.e.,

$$\frac{\Gamma}{2\pi U_o c} = \frac{C_{N_x} c}{8(z - z_i)_x} \quad (88)$$

where:

Γ = the vortex strength,

U_o = the free-stream velocity,

c = the radius of the cylinder,

C_{N_x} = the viscous normal force coefficient for all the viscous normal force behind station x (see Figure 2),

z = z-coordinate of right-hand real vortex,

z_i = z-coordinate of right hand image vortex,

the subscript x refers to conditions at the axial station x, and "normal" means perpendicular to the cylinder axis, x (i.e., in the direction of V). Equation (88) thus defines C_{N_x} as the drag coefficient due to profile, form or pressure drag, which, as previously described, may be used to approximate the cross-flow drag coefficient due to viscosity in equation (86). However,

in order to determine C_N one must know the strength, Γ , and location ($z - z_{ix}$) of vortices behind a cylindrical body. Again, much experimental work has been done in this area and analytic studies have begun to surface as well. Notable among these is the mathematical formulation of Sarpkaya (1968), who has attempted to describe the physical mechanism which controls the separation and growth of vortices behind a bluff body by the use of a sophisticated potential flow model. Sarpkaya presents his results in terms of a parameter κ , where κ lies between 1.0 and 2.0:

$$\Gamma = \kappa V^2 \Delta t \quad (89)$$

The characteristic time interval, Δt , is obtained from a consideration of the variation of pressure across the boundary layer at the point of flow separation, and $V = U_0 \sin \alpha$ as before. Vortex distribution behind the cylinder for a flow started impulsively from rest was calculated using a numerical iterative scheme, and early results compared favorably with the experimental data available at the time. Such data, however, is seriously lacking for the type of geometrical configurations depicted in Figure 1, and this would therefore suggest an important avenue of research to be pursued in future AMRL efforts.

In any case, it appears to be quite feasible to extend the analytic work developed in this report to include the viscous drag force which results from flow separation. Vortices of known (or assumed) strength may be placed on the lee side of any of the configurations thus far examined, and their respective potential functions added linearly to equation (28) for the uniform stream. The surface pressure distribution may then be readily calculated from Bernoulli's equation once the velocity field given by the complex velocity potential is known. And once the pressure distribution is known, the forces tending to displace the limb from its ejection position may be determined in a straightforward manner -- either purely by analytical means or by numerical methods if the mathematics gets too complicated.

SECTION VIII

CONCLUDING REMARKS

It has been shown in this report that one can approach the general problem of limb flailing during ejection by constructing a simplified model from which the aerodynamic forces exerted on an articulated body subjected to windblast may be reasonably estimated. This model can be progressively refined, made more sophisticated, and streamlined to provide important data for both experimental and numerical studies of human body dynamics. In the early form developed here, the body joints themselves have not been defined and it would be desirable to look into this in greater detail in order to assess the significance of finite length segments, end effects, three-dimensional contours and interactions which take place between the

limbs as a result of their joint connections. Along the same lines, the velocity \vec{U} must be viewed as the resultant of an outer flow that has undergone specific interactions with other body segments before it actually impinges upon a given limb, and this is an area which has not yet been explored. We mentioned it briefly at the end of Section II with respect to equation (11) and again after equation (55) in Section VI, when the presence of a torso was discussed relative to the angle of attack at which the fluid approaches the forearm.

In refining the theory, one might also back-track to examine more closely the consequences of other assumptions made in Section III. For example, the roughness of the surface over which the fluid flows (which may, in part, be due to the type of clothing being worn by the pilot) may lead to certain types of turbulent behavior that is not negligible. Similarly, at Mach numbers exceeding 0.5 compressibility effects should certainly be included at some point in the analysis. And finally, although the present report has concentrated specifically on the forearm, the theory could be developed in a more general form for straightforward extension to the other limbs of the body and to other body positions (e.g., holding a D-ring, one limb pressing against another - as the upper arm against the torso, etc.). The foundation for doing this lies in Section II (The Analytic Body Model) and in the generalized complex velocity potential of Section V.

For the immediate future, however, it would seem that the inclusion of flow separation effects as discussed in Section VII should be the next logical step in the mathematical analysis. Separation of the flow, together with the appearance of stagnation points in the fluid present themselves as first order effects responsible for the generation of limb-dislodging forces that result in flail injuries. The former gives rise to a pressure gradient that tends to drag the limb along with the air flow, and the latter results in a pressure gradient that tends to separate the limb from a surface with which it is in contact. Both of these effects are functions of the square of the velocity of the incident stream (see equations (89) and (76), for example) and so they become rather significant at speeds near sonic.

LIST OF SYMBOLS

\overline{AB}	Forearm Vector from Elbow Joint, A, to Wrist Joint, B.
A_P	Plan-Form Area = $2 \int_0^L R(x) dx$.
C_D	Total viscous drag coefficient.
$C_D(x)$	Local Drag Coefficient at station x.
C_{N_x}	Viscous Normal Force Coefficient for all the viscous normal force behind station x; Drag Coefficient due to profile, form, or pressure drag.
C_o	Bernoulli Constant.
C_m	Experimental Coefficients in the series expansion of C_D .
C_P	Surface Pressure Coefficient = $\frac{p - p_o}{\frac{1}{2} \rho U_o^2}$.
$C_{P_{\alpha=0}}$	Surface Pressure Coefficient due to fluid of velocity U impinging upon conical surface lying parallel to the stream.
D'	Effective Diameter = A_P/L .
E	The point $z = 0, y = c$.
G	The point $z = 0, y = -c$.
\overline{GE}	Chord line representing in end view the surface of intersection between the forearm and seat rest against which it is pressing.
L	Total length of arbitrary body.
P	Arbitrary point in space.
$R(x)$	Forearm cross-sectional radius at location x_o .
\vec{U}	Velocity of air stream approaching forearm = $U_1 \hat{i} + U_2 \hat{j} + U_3 \hat{k}$
U	x-component of \vec{U} , parallel to limb centerline.
U_o	Magnitude of \vec{U}

U_1	x'-component of \vec{U} .
U_2	y'-component of \vec{U} .
U_3	z'-component of \vec{U} .
V	y-component of \vec{U} , cross-flow velocity.
V^*	Local speed of sound.
a	Radius of circle tangent to y-axis = $a(x)$ for a cone, ($n = 0$).
c	Radius of free cylinder ($=R(x)$ for $n = 1$); Also, the coordinates of the intersection of the truncated cone with the y-axis, which constitutes the chord line \overline{GE} .
f	Cross-force per unit length of surface, not including the effects of flow separation.
$f_D(x)$	Viscous drag force per unit length of surface.
i	$\sqrt{-1}$; Also used as a superscript (from 1 to 15) to designate a particular body segment; Also used as a subscript to designate that the quantity is the image (e.g., a vortex image) of a quantity previously specified.
\hat{i}	Unit vector along the direction of x' .
j	Subscript for x-y-z axes, i.e., $j = x, y, z$.
\hat{j}	Unit vector along the direction of y' .
k	Subscript used to designate a particular body joint.
\hat{k}	Unit vector along the direction of z' .
ℓ	$ \overline{AB} $ = Length of forearm from elbow to wrist.
m	Subscript used as an index for the coefficients C_m .
n	Used as a general index for integers 0, 1, 2, ... Also used as a parameter in the complex velocity potential of Section V.
o	Used as a subscript to designate free-stream conditions
p	Fluid pressure

p_o	Free-stream pressure
$p_{\alpha=0}$	Surface pressure at any axial station when a truncated cone configuration lies with its axis parallel to an incident stream of fluid.
q	Magnitude of fluid velocity at a specified point in the flow, $q^2 = u^2 + v^2$
r	Radial coordinate in cylindrical coordinate system, $r^2 = y^2 + z^2$.
$\vec{r}_k(t)$	Radius vector drawn from the origin of an inertial coordinate system to the k'th body joint (1 = elbow, A; 2 = wrist, B).
t	Time coordinate.
u	Magnitude of fluid velocity in the y-direction at an arbitrary point in the flow.
v	Magnitude of fluid velocity in the z-direction at an arbitrary point in the flow.
\vec{v}	Velocity vector at an arbitrary point in the flow = a vector having components u and v along y and z , respectively.
w	Complex velocity potential = $\phi + i\psi$.
\bar{w}	Complex Conjugate of the velocity potential w ; = $\phi - i\psi$.
x	Coordinate axis constituting the center-line of the limb when it is free, or the line of contact between the limb and a solid surface.
x'	One of the coordinate axes of an inertial coordinate system.
x_o	A specific location along the limb.
y	Coordinate axis chosen so that the fluid approaches the limb parallel to the y -axis, in the x - y plane.
y'	A second coordinate axis in an inertial coordinate system.
z	Coordinate axis perpendicular to the x - y plane. x - y - z coordinate system is fixed to the limb.
z'	The third coordinate axis in the inertial coordinate system, x' - y' - z' .

α	Angle of attack of \vec{U} relative to limb: $\cos \alpha(t) = \hat{\lambda}_j^{(i)}(t) \cdot \hat{\lambda}_U$
	$\tan \alpha = \frac{V}{U}$
β	Forearm cone half-angle: $\tan \beta = \frac{dR(x)}{dx}$
ψ	Stream Function of the flow.
ϕ	Potential Function for the velocity of the flow: $\vec{v} = -\nabla\phi$.
$\hat{\lambda}_j^{(i)}(t)$	Unit vector defining the j'th coordinate axis ($j = x, y, z$) of the i'th body segment ($i = 1$ to 15) as a function of time.
$\hat{\lambda}_U$	Unit vector defining the direction of the air stream approaching the forearm: \vec{U}/U_0 .
η	$\ln(r_2/r_1)$, where r_2 and r_1 are intersecting radius vectors from points G and E, respectively, defining the point P in space. This is one of the coaxial coordinates.
κ	A parameter having a value between 1.00 and 2.00 and acting as a proportionality constant between the vortex strength, the square of the fluid velocity and a characteristic time interval.
μ	Fluid viscosity.
ρ	Fluid mass density.
θ	Azimuthal coordinate in cylindrical coordinate system, $\tan \theta = \frac{z}{y}$. The angle θ is measured counterclockwise from the positive y-axis.
ξ	$\theta_1 - \theta_2$, where θ_1 and θ_2 are the angles which r_1 and r_2 make, respectively with the y-axis. This is the second of the two coaxial coordinates.
δ	The angle $\frac{\pi}{2} \cot \theta$.
χ	The complex variable $y + iz = ic \cot \frac{\xi}{2} = re^{i\theta}$.
$\bar{\chi}$	The complex conjugate of χ ; $= y - iz = -ic \cot \frac{\xi}{2} = re^{-i\theta}$.
ζ	The complex variable $\xi + i\eta$.

$\bar{\zeta}$	The complex conjugate of ζ ; $= \xi - i\eta$.
∇	The Gradient operator.
∞	Designates infinity.
Γ	The strength of a vortex.
Σ	Designates a summation.
Δ	Designates a difference between the two quantities following.
π	3.14159.

COMPUTER PROGRAM FOR CALCULATING AND PLOTTING STREAM FUNCTIONS
DEFINED BY EQUATION (35) IN THE TEXT MATERIAL

APPENDIX

DLB,T350,CM100000,STCSB. L730533 BRUNGART
ATTACH,DISSPLA,ID=X654321,SN=AFIT.
LIBRARY,DISSPLA.
FTN.
LGO.
ONLINE.
"

```

PROGRAM FLOW(INPUT,OUTPUT,PLFILE=0)
COMMON YLAST,ZLAST
CALL COMPRS
CALL BGNPL(1)
CALL CROSS
CALL TITLE(1H,-1,"Y",1,"
                                Z",20,10.,7.)
CALL GRAPH(-5.,1.,0.,1.)
CALL CIRCLE
PI=355/113.
A=1
U=1
API=A*PI
APU=API*U
L=2
DO 6 K=1,2
DO 6 M=1,701,25
CALL BLNK1(8.9,10.0,0.,7.)
CALL BLNK2(0.,1.,0.,7.)
IF(L.EQ.2) CALL BLNK3(8.5,9.0,0.,7.)
F=-1
IF(K.EQ.2) F=1
PSIBASE=M*.005
KK=0
PSIU=PSIBASE+.01
PSIL=PSIBASE-.01
DO 5 I=1,200
Z=.025*I
DO 4 J=1,200
Y=.025*(J-1)*F
1 RSQ=Y*Y+Z*Z
FLY=API*Y/RSQ
FLZ=API*Z/RSQ
F2=TAN(FLZ)
F3=COSH(FLY)
F4=TANH(FLY)
PSI=APU*F2/((F3*F3)*(F4*F4+F2*F2))
IF(PSI.LT.PSIBASE) GO TO 4

```

	IF(((Z-1)*(Z-1)+Y*Y).LT.1) GO TO 4	000390
	IF(PSI.LT.PSIU.AND.PSI.GT.PSIL) CALL DRAW(Z,Y,KK)	000400
	IF(PSI.LT.PSIU.AND.PSI.GT.PSIL) GO TO 5	000410
4	CONTINUE	000420
5	CONTINUE	000430
	CALL RESET("BLNKS")	
	IF(L.EQ.2) GO TO 10	
	CALL MIXALF("GREEK")	
	IF(K.EQ.2) CALL MESSAG("(Y) =",5,9.0,ZLAST)	
	IF(K.EQ.2) CALL REALNO(PSIBASE,3,"ABUT","ABUT")	
	L=2	
	GO TO 6	
10	L=1	
6	CONTINUE	000440
	CALL ENDPL(0)	
	CALL DONEPL	
	STOP	000470
	END	000480
	SUBROUTINE DRAW(Z,Y,KK)	000490
	COMMON YLAST,ZLAST	
	Y=Y+5.	
	IF(KK.EQ.0) YLAST=Y	
	IF(KK.EQ.0) ZLAST=Z	
	IF(KK.EQ.0) CALL STRIPT(Y,Z)	
	CALL CONNPT(Y,Z)	
	KK=1	000550
	RETURN	000560
	END	000570
	SUBROUTINE CIRCLE	000580
	DIMENSION ZZ(101),YY(101)	000590
	DO 1 I=1,50	000600
	ZZ(I)=.04*I	000610
	ZZ(50+I)=2.-ZZ(I)	000620
	YY(I)=SQRT(1.-(ZZ(I)-1)*(ZZ(I)-1))	000630
	YY(50+I)=-YY(I)	000640
1	CONTINUE	000650
	DO 2 I=1,100	000660
2	CALL CONNPT(YY(I)+5.,ZZ(I))	
	RETURN	000680
	END	000690
"		

REFERENCES

- Allen, H. Julian and Perkins, Edward W., "A Study of Effects of Viscosity on Flow Over Slender Inclined Bodies of Revolution," NACA Technical Report Number 1048, 1951.
- Bartz, J. A., "A Three-Dimensional Computer Simulation of a Motor Vehicle Crash Victim - Phase I - Development of the Computer Program," Calspan Technical Report Number VJ-2978-V-1, July, 1971.
- Bartz, J. A., and Butler, F. E., "A Three-Dimensional Computer Simulation of a Motor Vehicle Crash Victim - Phase II - Validation of the Model," Calspan Technical Report Number VJ-2978-V-2, December, 1972.
- Brinkley, J. W., and Payne, P. R., "An Assessment of Aerodynamic Forces Acting on the Crewman During Escape," Advisory Group for Aerospace Research and Development, AGARD Conference Proceedings Number AGARD-CP-134, Paper A4, February, 1974.
- Clauser, Charles E., Tucker, Pearl E., McConville, John T., Churchill, E., Laubach, Lloyd L., and Reardon, Joan A., "Anthropometry of Air Force Women," Aerospace Medical Research Laboratory, Aerospace Medical Division, Air Force Systems Command, Technical Report Number AMRL-TR-70-5, April, 1972, Wright-Patterson Air Force Base, Ohio.
- Fleck, J. T., Butler, F. E., and Vogel, S. L., "An Improved Three-Dimensional Computer Simulation of Motor Vehicle Crash Victim," Calspan Technical Report Number ZQ-5180-L-1, July, 1974. Volume 1 - Engineering Manual, Volume 2 - Model Validation, Volume 3 - User's Manual, Volume 4 - Programmer's Manual.
- Fleck, J. T., and Butler, F. E., "Development of an Improved Computer Model of the Human Body and Extremity Dynamics," Aerospace Medical Research Laboratory, Aerospace Medical Division, Air Force Systems Command, Technical Report Number AMRL-TR-75-14, July, 1975, Wright-Patterson Air Force Base, Ohio.
- Garret, John W., and Kennedy, Kenneth W., "A Collation of Anthropometry," Aerospace Medical Research Laboratory, Aerospace Medical Division, Air Force Systems Command, March, 1971, Wright-Patterson Air Force Base, Ohio, Volumes I and II.
- Goldstein, Sydney, "Modern Developments in Fluid Dynamics," Oxford at the Clarendon Press, 1938, Volumes I and II.
- Hawker, F. W., and Euler, A. J., "Experimental Evaluation of Limb Flail Initiation and Ejection Seat Stability," in: Glaister, D. H., Ed., Biodynamic Response to Windblast, Advisory Group for Aerospace Research and Development, AGARD Conference Proceedings Number 170 (AGARD-CP-170), Paper B10, July, 1975.

- Kelly, Howard R., "The Estimation of Normal-Force, Drag, and Pitching-Moment Coefficients for Blunt-Based Bodies of Revolution at Large Angles of Attack," *Journal of the Aeronautical Sciences*, Vol. 21, No. 8, pp. 549-555, August, 1954.
- Mello, J. F., "Investigation of Normal Force Distributions and Wake Vortex Characteristics of Bodies of Revolution at Supersonic Speeds," *Journal of the Aerospace Sciences*, Vol. 26, No. 3, pp. 155-168, March, 1959.
- Milne-Thomson, L. M., "Theoretical Hydrodynamics," New York, The MacMillan Company, Fourth Edition, 1960.
- Payne, Peter R., "On Pushing Back the Frontiers of Flail Injury," in: Glaister, D. H., Ed., Biodynamic Response to Windblast, Advisory Group for Aerospace Research and Development, AGARD Conference Proceedings Number 170 (AGARD-CP-170), Paper B9, July, 1975.
- Payne, Peter R., "Notes on the Initiation of Limb Flailing," Aerospace Medical Research Laboratory, Aerospace Medical Division, Air Force Systems Command, Technical Report Number AMRL-TR-71-45, August, 1971, Wright-Patterson Air Force Base, Ohio.
- Sarpkaya, T., "An Analytical Study of Separated Flow About Circular Cylinders," ASME Paper Number 68-FE-15, Transactions of the American Society of Mechanical Engineers, *Journal of Basic Engineering*, 1968.